

Interference effect of beam splitter current in Iron-Pnictide superconductors

Abhisek Bag^{1,2,*} and Saptarshi Mandal^{1,2,†}

¹*Institute of physics, Bhubaneswar 751005, Odisha, India*

²*Homi Bhabha National Institute, Mumbai 400 094, Maharashtra, India*

(Dated: September 16, 2024)

We consider a Cooper pair beam splitter for Iron-Pnictide superconductor and calculate the entangled electron-hole current. We investigate the interplay of various physical parameters such as doping at electron and hole pockets as well as non-zero nesting between the electron and hole pocket. We find that in the absence of magnetic order, the current due to hole pocket and electron pocket add up ordinarily. However in the presence of magnetic ordering the two currents take part in characteristic interference effect to modify the resultant current significantly. This interference effect manifests itself in non-monotonous and oscillatory nature of beam splitter current. We investigate in details this non-monotonicity with the chemical potential as well as nesting vector $|\mathbf{q}|$. We also investigate the evolution of density of states with system parameters and correlate it with the beam-splitter current. Further we enumerate the relevant parameter space where the efficiency of such beam splitter set up is enhanced. Our finding can be useful in experimental determination or verification of co-existence phase in Iron-Pnictide superconductors and has potential applications in realizing quantum gates or switches.

I. INTRODUCTION

One of the fundamental aspect of quantum mechanics is the superposition principle which dictates that a quantum mechanical system can be described by a linear superposition of many orthogonal wave functions¹. This superposition principle yields an entanglement or correlations between different parts of the system. In recent times this fundamental aspect has been investigated in detail to construct entangled states having specific properties with application in teleportation, cryptology etc². To realize such entangled states many protocols have been proposed involving various mesoscopic system such as quantum dots, superconducting qubits etc³⁻⁶. However after preparing such entangled state one needs to confirm that the state is robust against decoherence^{7,8}. It is well known fact that various condensed matter system act as a source of such entangled many body states naturally. The existence of such entangled states is ubiquitous in various condensed matter systems such as the Cooper pairs in superconductivity⁹, ground state wavefunction for quantum spin liquid^{10,11}, resonating valence bond states¹² for certain magnetic systems etc.

Starting from the celebrated EPR paradox¹³ and culminating in Bell's inequality^{14,15}, entanglement is now an experimentally established reality¹⁶⁻¹⁸. In view of identifying such entangled states in the context of superconductivity, a Cooper pair beam splitter arrangement has been proposed for the first time in 19 and later on in other systems²⁰⁻²⁵. In these study it is proposed that the participating electrons and holes can be collected at two different leads after passing through two quantum dots kept at suitable distance. The collected electron and hole maintain their state of initial correlation or entanglement. Recently such studies has been extended to graphene²⁶ where a proximity induced superconductivity has been considered. There the authors have shown that the beam splitter current is increased in magnitude in

comparison to an ideal BCS superconductor in two dimensions. However the superconductivity in single layer graphene is not realized till now and the superconductivity in conventional BCS superconductor is realized at very low temperature limiting its practical application. Thus it motivates us to look for other system where such entangled beam splitter can be realized with naturally occurring unconventional superconductivity²⁷⁻³⁰ at high temperatures enabling us for practical applications.

In this study we have investigated the consequences of beam splitter arrangement for Iron-pnictide superconductors. Firstly we are motivated by the fact that this system is an example where various competing order parameters such as two superconducting pairing interactions and magnetic ordering exist simultaneously³¹⁻³⁵. Till date all the beam-splitter superconducting current studies are performed on systems containing only single pairing interaction. Thus consequences of many order parameters render it an interesting platform to study beam-splitter current. Secondly these systems are realized at quite high temperature for example at $\sim 50\text{K}$ for 1111- and 122- type systems³¹ thus providing relatively easier practical realisation. In fact we have found that the Cooper pair beam splitter current depends on the relative magnitude of chemical potential, two superconducting gaps and the magnetic order parameter in a nontrivial way. Though the exact expression for beam splitter current can not be obtained in the simultaneous presence of magnetic and superconducting order parameter like previous studies, our study offers numerous valuable consequences of the complexities of the system on beam-splitter current. We have also seen that unlike before, the beam-splitter current can be monotonically decreasing or an oscillating one depending on the relative shapes of the electron and hole pocket (associated with two superconducting gaps) as well as values of chemical potential at electron and hole pocket respectively. We attribute this to the interference effect from currents due

to hole and electron pocket. We also investigate the effect of the density of states of the system on the beam splitter current.

Our plan of presentation is the following. In section II we review the basics of Iron-pnictide superconductors^{36–38}, its model hamiltonian involving electron and hole pocket and brief description of superconducting and magnetic interaction between the hole and electron pocket in the system. After this, in section III, we present our model scheme of realising beam-splitter current in detail by calculating the entangled beam-splitter current in its full form for the Iron-pnictide system. We also enumerate all the assumptions and approximations needed for such calculation. In section IV, we first present the phase diagram of model hamiltonian discussed and the relevant range of parameters considered in the present study to explore the nature of beam splitter current. This includes all the relevant parts of the phase diagram. We present the beam-splitter current in the phase space as a whole at first. Then we discuss how beam splitter current varies with the distance between the two leads for various representative values of the parameters of the system such as chemical potential at electron and hole pocket, perfect and non-zero nesting etc. We also present the study of density of states and correlate it with the beam-splitter current. In Sec. V we briefly discuss the current when both the electrons are collected at the same dot and comment on the efficiency of the entangled beam-splitter current. Finally we conclude in section VI by summarising our results with a discussion.

II. MODEL

In FeAs, the relevant tight binding model which describes the superconductivity contains an itinerant electron system of two electronic orbitals due to two Fe atoms in an unit cell^{41–44}. The hybridization between the orbitals are such that it leads to a hole pocket centred at $(0,0)$ and an electron pocket centred at (π,π) in the folded zone scheme^{39,40}. Following earlier notations³⁹ we denote the fermions near $(0,0)$ by usual ‘ c ’ operator and for fermions near (π,π) by ‘ f ’. The model Hamiltonian can be written as follows,

$$H = H_0 + H_\Delta + H_m. \quad (1)$$

In the above H_0 denotes the non-interacting part of electron and hole pocket. H_Δ denotes superconducting pairing interaction and H_m signifies the magnetic pairing interaction. The details of these three terms are given below⁴⁰,

$$H_0 = \sum_k \epsilon_c(k) c_{k\alpha}^\dagger c_{k\alpha} + \sum_{k'} \epsilon_f(k') f_{k'\alpha}^\dagger f_{k'\alpha} \quad (2)$$

In the above $\epsilon_c = \mu_c - |k|^2/2m$ and $\epsilon_f = |k'|^2/2m - \mu_f$. Note that k appearing in ‘ c ’ is measured from the center of Brillouine zone and for ‘ f ’ fermion k' is measured

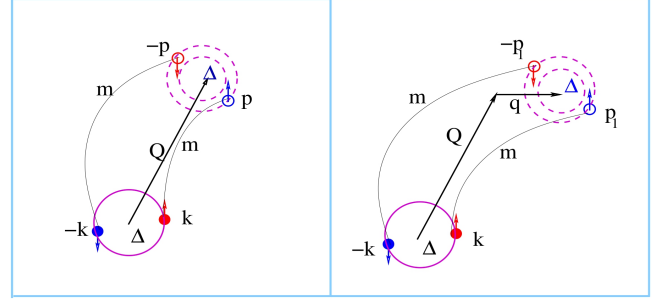


FIG. 1. The solid circle denotes hole pocket and the dashed circles denote electron pocket. The black lines connecting fermions at electron and hole pocket are responsible for magnetic ordering in the system. The left panel shows the case of perfect nesting and the right panel shows a non-zero nesting (finite q). Δ denotes the superconducting gap at the electron and hole pocket. The effect of chemical potential increases or decreases the relative size of electron and hole pocket which have been shown by two different dashed circles.

from (π,π) . Henceforth all the momentum indices associated with the ‘ f ’ fermions are understood as measured from (π,π) unless referred otherwise. Note that we have taken an isotropic mass at electron pocket and hole pocket. This assumption may be an approximated one without changing the qualitative aspect of the results found here. The superconducting pairing terms and the magnetic interactions are given by,

$$H_\Delta = \frac{1}{2} \sum_{k,p} V_{[\Lambda]}^{cf}(k,p) (c_{k\alpha}^\dagger c_{-k\beta}^\dagger f_{-p\beta'} f_{p\alpha'} + h.c) \quad (3)$$

$$H_m = -\frac{1}{4} \sum_{\delta p = \delta k} V_{[\Lambda]}^{sw}(p'p : kk') (f_{p'\alpha}^\dagger c_{p\beta} c_{k\beta'}^\dagger f_{k'\alpha'} + h.c) \quad (4)$$

Where $\delta p = p' - p$ and $\delta k = k' - k$ and $[\Lambda] = \alpha\beta\beta'\alpha'$ denotes combined spin indices. In the above, Eq. 3 describes the effective pairing interactions in the Iron-pnictide system which arises due to the inter-band hopping between electron and hole band³⁹. The magnetic interactions as denoted in Eq. 4 come from the inter-band density-density interactions. The pairing interaction $V_{\alpha\beta\beta'\alpha'}^{cf}(k,p) = V_{k,p}^{sc}((i\sigma^y)_{\alpha\beta}(i\sigma^y)_{\beta'\alpha'}^\dagger)$ and the magnetic interaction $V_{\alpha\beta\beta'\alpha'}^{sw}(p'p : kk') = V_{p'p:kk'}^{sw} \sigma_{\alpha\beta} \cdot \sigma_{\beta'\alpha'}^\dagger$. Following earlier convention^{39,40}, we define the superconducting pairing order parameter and magnetic order parameter as $\Delta_c(k)_{\alpha\beta} = (i\sigma^y)_{\alpha\beta} \sum_p V_{kp}^{sc}(i\sigma^y)_{\beta'\alpha'}^\dagger \langle f_{-p\beta'} f_{p\alpha'} \rangle$, $(m_q)_{\alpha\beta} = -\frac{V_{sw}}{2} \sum_p \sigma_{\alpha\beta} \cdot \sigma_{\beta'\alpha'}^\dagger \langle c_{p\beta}^\dagger f_{p+q\alpha'} \rangle$. $\Delta_f(k)_{\alpha,\beta}$ is defined identically as $\Delta_c(k)_{\alpha,\beta}$. Note that the momentum index q appearing in the definition of magnetic order parameter m_q refers a small deviation of the centre of hole pocket from (π,π) . This is to account for the fact that when $q = 0$, magnetic order is found to be zero which will be discussed again Sec. IV. We use the above definitions of mean field order parameters to perform a meanfield decomposition of the four fermion interactions

as given in Eq. 3 and Eq. 4. The resulting Hamiltonian obtained is written in the following matrix form,

$$H = \sum_{k\alpha\beta} \bar{\Psi}_{k\alpha} \hat{H}(k)_{\alpha\beta} \Psi_{k\beta} - 2 \frac{\Delta_c \Delta_f}{V_{SC}} + 2 \frac{m_{\alpha\beta}^* m_{\alpha\beta}}{V_{SD}}, \quad (5)$$

where the four component Nambu spinor is, $\bar{\Psi}_{k\alpha} = (c_{k\alpha}^+, c_{-k\alpha}, f_{p\alpha}^+, f_{-p\alpha})$ with $p = k + q$ and the Hamiltonian matrix $\hat{H}(k)_{\alpha\beta}$ which we write in short $\hat{H}_{\alpha\beta}$ has the form,

$$\hat{H}_{\alpha\beta} = \begin{pmatrix} \epsilon_c(k)_{\alpha\beta} & \Delta_c(k)_{\alpha\beta} & m_{q\alpha\beta}^* & 0 \\ -\Delta_c(k)_{\alpha\beta} & -\epsilon_c(k)_{\alpha\beta} & 0 & -m_{q\alpha\beta}^* \\ m_{q\alpha\beta} & 0 & \epsilon_f(p)_{\alpha\beta} & \Delta_f(p)_{\alpha\beta} \\ 0 & -m_{q\alpha\beta} & -\Delta_f(p)_{\alpha\beta} & -\epsilon_f(p)_{\alpha\beta} \end{pmatrix} \quad (6)$$

Note that initially the superconducting pairing interaction (as given in Eq. 3) is defined such a way that a hole of momenta k can interact with another electron of momenta p belonging to electron pocket centred around $(\pi, -\pi)$. However in the final expression in Eq. 5 another simplification has been performed where a hole with momenta k take part in pairing interaction with another electron at hole pocket with momenta k only. The index q signifies that the electron pocket is no longer around $(\pi, -\pi)$ but rather around $(\pi, -\pi) + q$ to take into account finite magnetic order parameter. In the above we have accounted for two different kind of magnetic order parameter with the following definitions. If $\alpha = \beta, m_{\alpha,\alpha} = m_1$ and for $\alpha \neq \beta, m_2 = m_{\alpha,\beta}$. Following earlier study^{39,40} we choose $m_1 = m, m_2 = 0$ in our study without loss of generality. One can easily obtain the spectrum after diagonalizing the 8×8 matrix in Eq. 6, the detail expressions for the eigenvalues are given in Appendix B. We obtain the ground state energy by filling the negative energy eigenstates which correspond to the vacuum of new Bogoliubov quasi-particles. Along with the constant terms the ground state energy can be written as $E_{min} = -\mathcal{E}_{kq+} - \mathcal{E}_{kq-} - \frac{\Delta_c \Delta_f}{V_{SC}} + 2 \frac{m^2}{V_{SD}}$. Where $\mathcal{E}_{kq\pm} = \sqrt{\mathcal{P}_k \pm \sqrt{\mathcal{Q}_k}}$ where \mathcal{P}_k and \mathcal{Q}_k are functional of $\epsilon_c(k), \epsilon_f(p), \Delta_c, \Delta_f, m$ and their detail expressions are given in Appendix B. We first derive the self consistent equations for the meanfield order parameter by minimizing Eq. 5 with respect to appropriate meanfield order parameters. Next we evaluate those meanfield order parameters self-consistently with the help of eigenvectors obtained after diagonalizing Eq. 6. Once the meanfield order parameters values are obtained we use them to calculate the beam-splitter current. Note that we evaluate the meanfield order parameters at zero temperature and thus beam-splitter current refers to zero temperature study only. Now we move on briefly to describe the beam-splitter current calculation.

III. MODEL FOR BEAM SPLITTER GEOMETRY

Having described the basic model of superconductivity and coexistence of magnetic order with it in Iron-Pnictides we now elaborate on the beam splitter arrangement designed for such system. Our idea of entangled Cooper pair splitter is similar to the seminal work of¹⁹ where for the first time an outline of Cooper pair entangled beam splitter arrangement was introduced. In Fig. 2, we present a schematic diagram of entangled beam-splitter arrangement. It is expected that electrons in a superconducting Copper pair in an iron-pnictide material will be tunneling through two spatially separated quantum dots where each quantum dot allows one electron (among the two participating electrons in a superconducting pair). However we note that in previous studies^{19,26} a superconducting eigenstate is of the form $\gamma_k = u_k c_{\uparrow,k} + v_k c_{\downarrow,-k}^\dagger$ and hence there are possibilities of only two kind of currents. The first one is where the electron with spin up and momentum k enters into one of the quantum dot and the other enters into the remaining quantum dot. This current is defined as \mathcal{I}_1 and it shows characteristic oscillations with the separation between the quantum dots. The second kind of current is obtained where both the electrons enter through the same dot with some time gap in between them. This current is defined as \mathcal{I}_2 and it is found to be a constant for a given set of parameters. The ratio $\mathcal{I}_1/\mathcal{I}_2$ signifies the efficiency of the beam splitter current so as to differentiate the \mathcal{I}_1 from \mathcal{I}_2 . In the present scenario an eigenstate in superconducting phase is of the form $\gamma'_k = u_k c_{\uparrow,k} + v_k c_{\downarrow,-k}^\dagger + u'_k f_{\uparrow,k} + v'_p f_{\downarrow,-p}^\dagger$. Hence in our case the current \mathcal{I}_1 is obtained by considering the two participating entangled Cooper pair, one due to c -fermion and another due to f -fermion. Note that we do not consider the current due to tunneling of a c and f fermion which participate in magnetic ordering. The current due to such event vanishes due to singlet nature of the quantum dot and metallic lead.

The current \mathcal{I}_1 is expected to happen once the quantum dots are kept in the Coulomb blockade regime such that it is energetically unfavorable to accommodate two electrons at the same quantum dot. Finally once two spatially separated electrons enter into two separate quantum dots, they are collected by two fermi liquid leads (represented by L_1 and L_2 in Fig. 2). However to realize such entangled electrons to be separated the chemical potentials of the superconducting materials (μ_s), quantum dots (ϵ_1 and ϵ_2) and also the leads (μ_1 and μ_2) are to be kept in certain conditions. While the chemical potentials at the two fermi liquid leads can be kept equal generally, the chemical potentials of the two quantum dots should be such that $\epsilon_1 + \epsilon_2 = 2\mu_s$ corresponding to two particle Breit-Wigner resonance⁴⁵. The transport of two entangled electron or hole pairs from the quantum dots to the leads can be achieved by applying a bias volt-

age $\Delta\mu = \mu_s - \mu_l$. We here outline the calculation of \mathcal{I}_1 and the details about \mathcal{I}_2 is discussed in Sec. V and in Appendix-A.

It is natural to expect that once the electrons tunnel from the superconductor to quantum dots, they interact with the already existing electrons at the quantum dots and this might lead to decoherence between the two separated electrons. One way to avoid this is to work in the co-tunneling regime where the number of electrons in the quantum dots are fixed and also the resonant level ϵ_1, ϵ_2 are not occupied. The probability of interaction can also be reduced if the entered electrons spend less time in the quantum dots and this can be achieved by having $|T_{SD}| < |T_{DL}|$. Also the temperature of the superconductor and the quantum dots should be such that $\Delta\mu > K_B T$ as this will ensure that the stationary occupation due to the coupling to leads is exponentially small. The complete Hamiltonian for the proposed

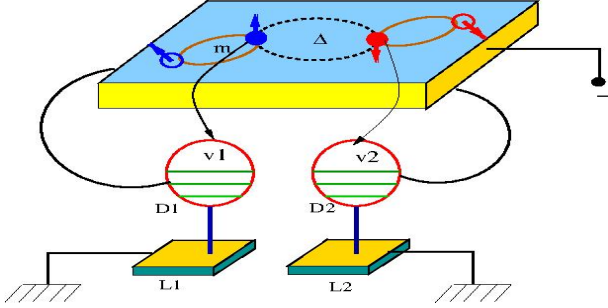


FIG. 2. Cartoon picture of Cooper Pair Beam Splitter set-up for Iron-pnictide superconductor. The blue rectangular slab with yellow border represents the superconductor and a Bogoliubov quasiparticle has been drawn schematically on it. The two filled circles represent fermions participating in superconducting order parameter Δ and the magnetic order is represented by the coupling between one filled circle and one empty circle. The superconducting slab is connected to two quantum dots (D1 and D2) by black lines. Each quantum dot is finally connected to fermi (metallic) leads L1 or L2. The direction of the current is indicated by the green arrows.

beam splitter device thus contains the intrinsic Hamiltonian of the Iron-pnictide materials, two quantum dots and two fermi (metallic) liquid quantum leads. In addition to the intrinsic Hamiltonians mentioned above, it also involves the tunneling Hamiltonians between the superconductor and the quantum dots and between the quantum dots and the leads. The complete Hamiltonian represented by H_{Tot} for the beam splitter set up thus becomes,

$$H_{tot} = H_S + \sum_l H_{D,l} + \sum_l H_{L,l} + H_{SD} + H_{DL}. \quad (7)$$

In the above the first three terms indicate the intrinsic Hamiltonians of superconducting material, quantum dots and lead respectively. Henceforth the subscript S, D, L will be used for the superconductor, quantum dots and the leads respectively. 'l' denotes the number of leads and

quantum dots which can take values 1 and 2. The term H_{SD} and H_{DL} denote the tunneling Hamiltonians from superconductor to quantum dots and quantum dots to leads respectively. Below we give in detail the complete expressions of each terms in Eq. 7.

$$H_S = \sum_{k\sigma} [\mathcal{E}_{kq} + \gamma_{kq\sigma}^c \gamma_{kq\sigma}^c + \mathcal{E}_{kq} - \gamma_{kq\sigma}^f \gamma_{kq\sigma}^f] + \mathcal{E}_0 \quad (8)$$

$$H_{Dl} = \sum_{\sigma,l} \epsilon_l d_{l\sigma}^\dagger d_{l\sigma} + U n_{l\sigma} n_{l-\sigma}, \quad (9)$$

$$H_{Ll} = \sum_{k\sigma} \epsilon_k a_{lk\sigma}^\dagger a_{lk\sigma} \quad (10)$$

$$H_{SD} = \sum_{l\sigma,i} g_i T_{SD}^i d_{l\sigma}^\dagger \Psi_\sigma^i(r_l) + h.c \quad (11)$$

$$H_{DL} = \sum_{lk\sigma} T_{DL} a_{lk\sigma}^\dagger d_{l\sigma} + h.c \quad (12)$$

In the above $\mathcal{E}_{kq\pm}$ denotes the energy of Bogoliubov quasi-particle excitations discussed before. $\gamma_{kq\sigma}^c$ and $\gamma_{kq\sigma}^f$ are creation operators for Bogoliubov quasi-particle. \mathcal{E}_0 denotes the constant energy not important to our consideration and does not affect the beam-splitter arrangements. ϵ_l denotes the energy levels of quantum dots and U refers the interaction energy if a given energy level of the quantum dot is occupied by two electrons of opposite spins. ϵ_k describes the energy of the Bloch states of fermi liquid leads. T_{SD}^i is the tunneling amplitude between superconductor and i 'th quantum dots and Ψ^i represents a state of an electron/hole arriving at i 'th quantum dot. g_1 and g_2 can take value 0 or 1 depending on which kind of quasi-particle is taking part in the Andreev process. We note that $g_1 \neq g_2$ signifies two types of quasi particles can not be present simultaneously in a pair of dots. Lastly T_{DL} denotes the tunneling amplitude between quantum dots and fermi liquid leads.

A. Current: via different dots

Having provided a brief introduction on Iron-pnictide system in Sec. II and the beam-splitter set up in detail in Sec. III, we now outline the important steps in evaluating beam-splitter current which are finally measured at the fermi liquid leads. The current due to electrons coming from superconductor and finally reaching to lead via quantum dots are represented by¹⁹ $I = 2e \sum_{f,i} W_{f,i} \rho_i$ where $W_{f,i} = 2\pi |\langle f | T_{\epsilon_i} | i \rangle|^2 \delta(\epsilon_f - \epsilon_i)$ is the transition rate from an initial state of electron $|i\rangle$ to a final state $|f\rangle$ which is discussed below in detail and ρ_i denotes the electron density. Here $T(\epsilon_i)$ is the on-shell transmission matrix and is given by⁴⁶ $T(\epsilon_i) = H_T \frac{1}{(\epsilon_i + i\eta - H)} (\epsilon_i - H_0)$. In the above H_0 denotes the Hamiltonian for superconductor ($H_0 = H_S$) and H_T denotes the successive tunneling from superconductor to quantum dots and subsequently from quantum dots to leads. $H = H_C$, is the total Hamiltonian. As $H_T \ll H_0$, we can expand the

denominator in appropriate power series and we obtain in $\eta \rightarrow 0$ limit,

$$\begin{aligned}
T(\epsilon_i) &= H_T \frac{1}{(\epsilon_i + i\eta - H_0 - H_T)} (\epsilon_i - H_0) \\
&= H_T \frac{1}{\tilde{H}_0 \left(1 - \frac{H_T}{\tilde{H}_0}\right)} (\epsilon_i - H_0), \quad \tilde{H}_0 = \epsilon_i + i\eta - H_0 \\
&= H_T \frac{1}{\tilde{H}_0} \left(1 + \sum_n \left(\frac{H_T}{\tilde{H}_0}\right)^n\right) (\epsilon_i - H_0) \\
&= H_T + H_T \sum_{n=1}^{\infty} \left(\frac{H_T}{\epsilon_i + i\eta - H_0}\right)^n \quad (13)
\end{aligned}$$

In the last step we have employed the fact that $\eta \rightarrow 0$ and summation over 'n' runs from zero to infinity as indicated. We note that $\langle f|T(\epsilon_i)|i \rangle$ denotes two step processes such that $\langle f|T|i \rangle = \langle f|T'|f' \rangle \langle f'|T''|i \rangle$ where T'' denotes the tunneling from superconductor to quantum dots and T' denotes the tunneling from quantum dots to leads. The expressions for T' and T'' are obtained as¹⁹,

$$T'' = \frac{1}{i\eta - H_0} H_{SD} \frac{1}{i\eta - H_0} H_{SD} \quad (14)$$

$$T' = H_{DL} \sum_{n=0}^{\infty} \left(\frac{H_{DL}}{i\eta - H_0}\right)^{2n+1}. \quad (15)$$

In arriving at the above form of the tunneling amplitude we have considered the fact that $|T_{SD}| < |T_{DL}|$ and while the electron can come and go from the dot to lead many times, there is no possibility of an electron to go back from quantum dot to superconductor¹⁹. We note that $|i \rangle = |0\rangle_S \otimes |0\rangle_D \otimes |\mu_l\rangle_l$ where the subscript S, D, l are used to denote the initial states of superconductor, quantum dots and leads respectively. The states $|f \rangle = |LL\rangle, |f' \rangle = |DD\rangle$ denotes the final states of leads and quantum dots respectively which are due to arrival of electrons from superconductor and hence represents a state with higher number of electrons and can be written as,

$$|f \rangle = \frac{1}{\sqrt{2}} (a_{1p\uparrow}^+ a_{2q\downarrow}^+ - a_{1p\downarrow}^+ a_{2q\uparrow}^+) |i \rangle, \quad (16)$$

$$|f' \rangle = \frac{1}{\sqrt{2}} (d_{1\uparrow}^+ d_{2\downarrow}^+ - d_{1\downarrow}^+ d_{2\uparrow}^+) |i \rangle. \quad (17)$$

Taking into account the orthogonality of states of different occupation numbers and momentum conservation, we obtain $\langle f|T'|f' \rangle = \langle i|a_{2q\downarrow} a_{1p\uparrow} T' d_{1\uparrow}^+ d_{2\downarrow}^+ |i \rangle$. We now turn to simplify $\langle f'|T''|i \rangle = \frac{1}{\sqrt{2}} \langle i|(d_{2\downarrow} d_{1\uparrow} - d_{2\uparrow} d_{1\downarrow}) T'' |i \rangle$, which denotes Andreev process. It may happen that in the process of transport one electron with a particular spin(say up) arrives at the quantum dot from the superconductor but an electron with opposite spin(say down) may travel forward from the same dot to the lead but we forbid that process. We want processes such as $|SS\rangle \rightarrow |DS\rangle \rightarrow |DD\rangle$ and $|SS\rangle \rightarrow |SD\rangle \rightarrow |DD\rangle$ simultaneously. Such that entangled pair of electrons from

the superconductor(SS) get transported to two dots (DD) and move forward to the respective leads, because we avoid spin flipping. Where, $|SD\rangle = \gamma_{k\sigma}^+ d_{l-\sigma}^+ |i \rangle$. We ensure that $H_{S_1 D_1}$ selects one electron of the entangled pair to dot 1 and $H_{S_2 D_2}$ selects the other electron of the entangled pair to dot 2. A little algebra gives us the following expression,

$$\mathcal{I}_1 = \mathcal{C}_0 \mathcal{I}_D, \quad \mathcal{I}_D = \left(\sum_k \mathcal{A}_k \cos(k_f \delta r) \right)^2 \quad (18)$$

In the above δr represents the separation between two quantum dots. For detailed derivation of the above equation we refer Appendix-A. In the above $\mathcal{C}_0 = \frac{e\gamma_s^2 \gamma}{4\pi^2 \nu_s^2 [(\epsilon_1 + \epsilon_2)^2 + (\gamma^2/4)]}$ and denotes a constant depended on system specification. Here $\gamma = \sum \gamma_l; l = 1, 2$ and $\gamma_l = 2\pi \nu_l T_{DL}^2$ (we remind that $l = 1, 2$ denote leads). Also $\gamma_s = 2\pi \nu_s T_{SD}^2$, where ν_s, ν_l are density of states per spin at lead and superconductor respectively. To understand the consequences of the magnetic order parameter and superconducting pairing, we expand the expressions of \mathcal{A}_k below.

$$\mathcal{A}_k = \sum_{i=1,3}^{\alpha=c,f} \frac{u_{i,k}^\alpha u_{i+1,k}^\alpha - u_{i,-k}^\alpha u_{i+1,-k}^\alpha}{E_{ikq}} \quad (19)$$

In the above we have used $E_{1kq} = \mathcal{E}_{kq+}$ and $E_{3kq} = \mathcal{E}_{kq-}$. We note that in the absence of magnetic ordering the first and third term vanishes and we are left with two copies of superconducting pockets. In the presence of magnetic ordering all the four terms are present and consequently the amplitude of the beam-splitter current is modified significantly. As an electron or hole has to participate simultaneously to the formation of superconducting pairing as well as in magnetic ordering the amplitude of beam-splitter current is expected to be modified significantly. In the following, we investigate \mathcal{I}_D instead of the full current \mathcal{I}_1 as in Eq. 18 following earlier convention²⁶, which anyway is different only by a constant factor. We evaluated \mathcal{I}_D numerically and plotted against $k_f \delta r$ for different values of system parameters such as doping at electron and hole pocket, nesting vectors etc in the next section. In the following text we simply refer \mathcal{I}_D as the beam-splitter current. We also note that all our calculations are done at zero temperature.

IV. NUMERICAL RESULTS

We numerically solve the self consistent equations for order parameters to get the corresponding values and use them to compute the current as given in Eq. 18. Before presenting our results for the beam-splitter current we briefly discuss the phase diagram in \mathbf{q} vs μ plane where \mathbf{q} is the nesting vector and μ denotes the amount of doping in the hole or electron pocket. In Fig. 3 we present the phase diagram obtained after numerically solving the

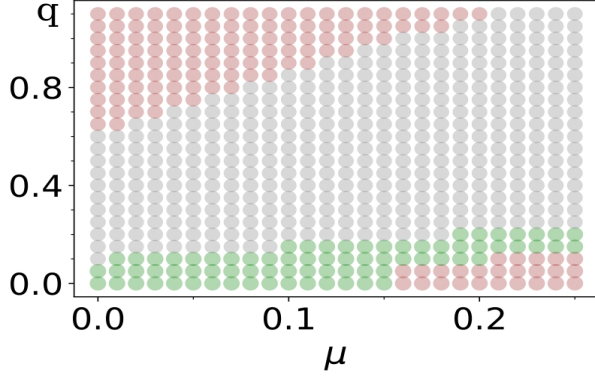


FIG. 3. The phase diagram in \mathbf{q} - μ plane. The region filled with green filled circle denotes magnetic phase. The pink colored region denotes superconducting phase and grey colored region is the co-existence phase where superconducting and magnetic order co-exist.

self-consistent equations as described in Sec. II. The main feature of the phase diagram is that the co-existence phase which is the salient aspect of Iron-pnictide superconducting system exists for specific values of \mathbf{q} and μ . For example, to get the co-existence phase a finite nesting (finite values of \mathbf{q}) is needed as evident from Fig. 3. Also for very large values of \mathbf{q} , the coexistence phase ceases to exist yielding only superconducting phase. Here we briefly compare our numerical phase diagram to that obtained in reference 40. For zero nesting case, i.e. $\mathbf{q}=0$ we observe a transition from pure SDW to pure SC phase around 0.15 doping or the mismatch factor between the hole and electron pocket as previously obtained at zero temperature⁴⁰. It is important to note that μ is same as the δ_0 considered there. Also for $\mathbf{q} \neq 0$ case, the transition happens at larger values of μ than which is obtained at $\mathbf{q}=0$. Later we present further comparison of density of state calculation with the previous results in Sec. IV C which has been used to benchmark our result. In our numerical analysis, we have taken $V_s = 2.5$ and $V_m = 3.0$ and chemical potential is initially kept at 1.7 which determines the initial pocket sizes (i.e. before doping) to standardise our results with the previous work⁴⁰. Value of chemical potential is taken in the units of meV. It may be noted that in Eq. 2 \mathbf{k}^2 is to be understood as $\hbar^2 \mathbf{k}^2$. We know that using value of $|\mathbf{k}| \sim 2\pi/a$ where a is of the order of Angstrom, one finds $\frac{\hbar^2 \mathbf{k}^2}{2m}$ of the order of meV. In our numerical calculation we have taken $m_c = m_f = 1$ in Eq. 2 (instead of 0.51 meV) which implies that the lattice spacing a to be appropriately scaled to a higher value $a \rightarrow \sqrt{2.0}$ Angstrom (approximately) which is more realistic. The value of \mathbf{q} is to be understood of the order of $2\pi/a$. Value of Δ is to be understood in meV as well. As we have plotted \mathcal{I}_D instead of \mathcal{I}_1 , the unit of \mathcal{I}_D is meV^{-2} where as the unit of \mathbf{q} is Angstrom^{-1} . Further we have confirmed the previous finding that the sign change of the superconducting gaps between the hole and electron pocket i.e. $\Delta_c = -\Delta_f$ happens only when V_s is positive.

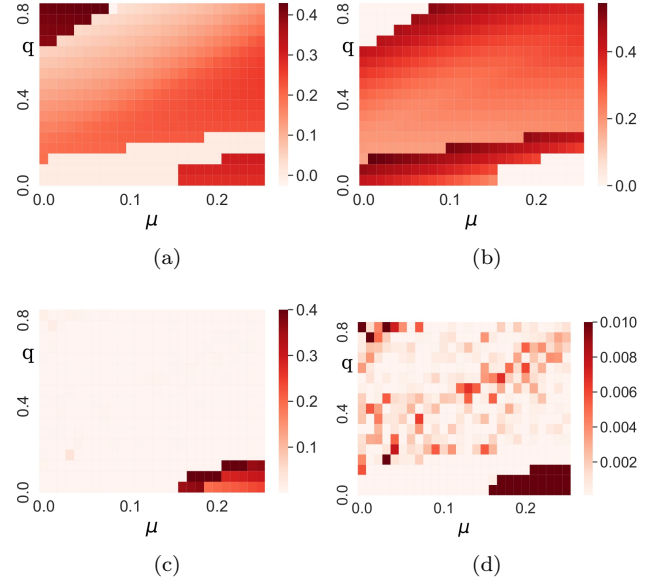


FIG. 4. In panel (a) density plots for the Δ (superconducting pair) is shown. In panel (b) density plot of m (magnetic order parameter) is presented. In $q-\mu$ plane in the upper left and right panel respectively. In panel (c) density plot for beam-splitter current is presented in $q-\mu$ plane. Finally in panel (d) zoomed in version of beam-splitter current is shown to illustrate the oscillating nature of current.

To complete the understanding of phase diagram given in Fig. 3, we have plotted the amplitude of superconducting gap Δ and magnitude of magnetic order parameter \mathbf{m} in $\mathbf{q}-\mu$ plane in Fig. 4 (a) and (b) respectively. These clearly shows that only in the coexistence phase both the parameters are finite. We refer reference⁴⁰⁻⁴⁴ for more details on the mechanism of magnetic and superconducting ordering and the phase transitions for the interested reader.

Finally In Fig. 4 (c), we plotted the beam-splitter current in the $\mathbf{q}-\mu$ plane for $k_f \delta r = 0$ which clearly shows that in the superconducting phase at low \mathbf{q} regime current is significantly higher than in the coexistence phase. However in the coexistence phase the current is finite though lower in magnitude than that in pure superconducting phase. If we zoom in the current in coexistence phase as given in Fig. 4 (d), we find that the current is higher in some region and lower in some region depending on the values of \mathbf{q} and μ . In subsequent discussion we describe in detail how the current behaves as a function of $k_f \delta r$ for various fixed values of μ and \mathbf{q} .

A. Comparison of beam-splitter current for electron doped vs hole doped

Here we discuss how the current varies with distance between the leads (which we denoted as δr) when the chemical potential at hole and electron pocket are var-

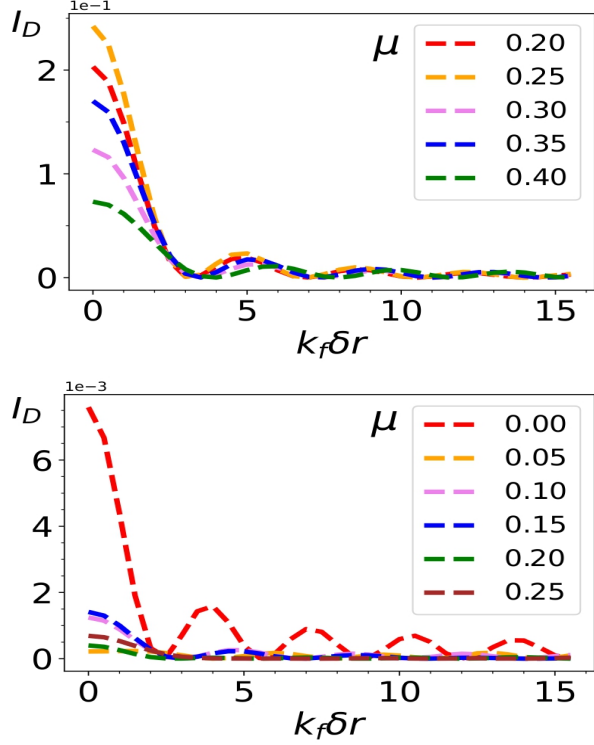


FIG. 5. Beam splitter current is plotted for identical shapes of electron and hole pocket for different chemical potential. Here the chemical potential μ refers both the electron and hole doping. In the upper panel we plotted current for perfect nesting $\mathbf{q}=0$ and in the lower panel we have plotted current for finite nesting $\mathbf{q}=0.4$.

ied independent of each other. First we discuss what happens when there is perfect nesting such that $\mathbf{q} = \mathbf{0}$. In this case we note that there is no co-existence phase and magnetic order parameter does not exist. As a result there is no such entanglement between the hole and electron pocket though the superconducting gap in hole pocket is determined by the electrons at electron pocket through self-consistent equations. Throughout this article we have taken identical shape of the hole and electron pocket which is circular in our case, for simplicity. In the upper panel of Fig. 5 we plotted the current when the nesting vector $|\mathbf{q}|$ is zero and in the lower panel we have plotted for a finite nesting vector \mathbf{q} . Due to symmetry the beam current does not depend on the nature of doping whether it is electron doped or hole doped. The chemical potential μ in Fig. 5 represents μ_c . The identical plots are obtained for $-\mu$ which represents electron doping i.e μ_f . This is consistent with the symmetry of the system. In both the cases, however, the current is non-linear for a given value of $k_f \delta r$. For example when μ is increased from 0.2 to 0.25 in the upper panel of Fig. 5, we find an increase in current but further increase in μ to 0.4 causes a decrease in current for perfect nesting. Similar observation holds for finite nesting as well. The main difference between the upper and lower panel of the Fig.

5 is that the magnitude of current is decreased by two decimal magnitude for finite \mathbf{q} . Noting that a finite \mathbf{q} represents a co-existence phase having magnetic and superconducting order parameter both, it can be concluded that existence of magnetic order parameter is the main reason behind this decrease of current. To understand how this happens we note the form of \mathcal{A}_k given in Eq. 19 can be written as $\mathcal{A}_{k,c} + \mathcal{A}_{f,k}$ where c, f denote the contribution from electron and hole pocket respectively. We notice that in pure superconducting phase the current due to hole and electron pocket is additive and there is no cross terms. On the other hand in the presence of magnetic order the magnitude of $\mathcal{A}_{c,k}$ or $\mathcal{A}_{f,k}$ is decreased individually due to normalization factor now spread over both kind of fermions. Also in the coexistence phase the cross terms in the expression \mathcal{A}_k does not vanishes, i.e there is quantum entanglement between the hole current and electron current which results in quantum interference effect to set in. These two facts make the current decreased in comparison to pure superconducting phase. However the property which is common in both the cases (finite and zero nesting) is that current is oscillatory or non-monotonous at a given $k_f \delta r$ with respect to varying μ . While the reason of oscillations for zero nesting may be attributed to density of states variation with the system parameters, the oscillations at finite nesting comes from quantum interference effect due to entanglement between hole and electron pocket.

B. Variations of beam splitter current with respect to nesting vector \mathbf{q}

Having discussed the effect of doping at electron and hole pocket on beam current, we move on to discuss how the current behaves for non-zero nesting vector for different sizes of the hole and electron pocket. A non-zero nesting vector imply that if the electron pocket is situated at $(0,0)$, the hole pocket is situated at $\mathbf{Q} + \mathbf{q}$ where $\mathbf{Q} = (\pi, \pi)$ and \mathbf{q} is called nesting vector. We also note that for non-zero \mathbf{q} , magnetic ordering is present along with superconducting ordering. In Fig. 6 upper panel we have taken electron and hole pocket to be of identical size i.e no doping and plotted current for representative value of \mathbf{q} . As can be seen, in this case also, the current varies in a non-linear fashion with respect to \mathbf{q} at given values of $k_f \delta r$. In the lower panel we have plotted the current for hole doped system for various values of \mathbf{q} (for electron doped system, the results is identical). This implies a situation where one pocket is bigger than the other. In this case also the beam splitter current is non-linear with respect to \mathbf{q} . However for both the cases we observe that as the magnitude of nesting vector increases, the beam current decreases and there is an oscillation for intermediate values of nesting vector. This oscillation arises due to same reason explained in previous section.

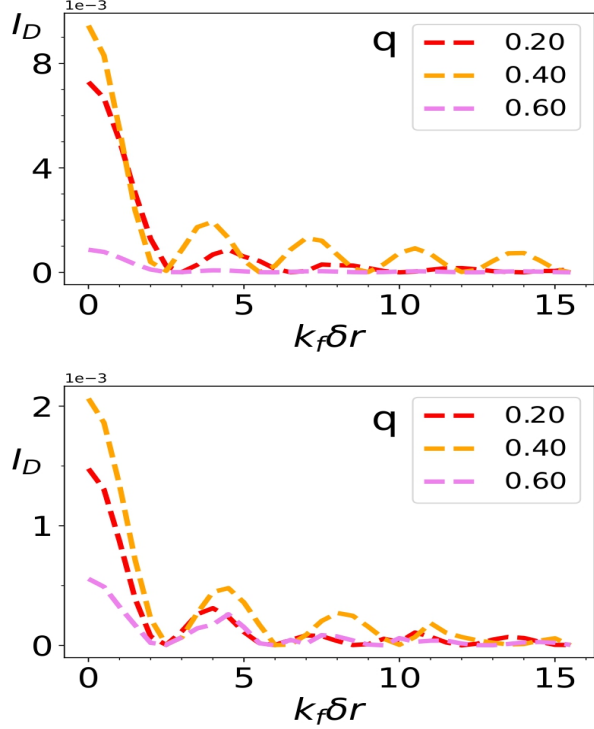


FIG. 6. In the upper panel beam-splitter current is plotted for equal size hole and electron pocket (i.e $\mu = 0$). In the lower panel current is plotted for electron pocket bigger than hole pocket i.e for case of electron doped system. We have taken $\mu = 0.2$. The current is same if the hole pocket is doped by same amount. For both the cases, different colors represent different amount of finite nesting for which currents have been plotted.

C. Oscillations of beam-splitter current

In the previous two sections we have explained that there are characteristic oscillations of beam splitter current. For a given $k_f \delta r$ the current depends on the chemical potential or doping in a non-linear way. To show these oscillations in a more transparent way, in Fig. 7, we plot the beam splitter current for different doping as well as for different nesting vectors at $k_f \delta r = 0$. In the panel (a) we plot the current for a given value of $k_f \delta r$ for $q = 0$. Evidently current decreases with respect to μ as expected but for intermediate ranges of μ current increases. This is the result of interdependence of superconducting pairing order (Δ_c and Δ_f) on electron and hole pocket as discussed before. We note that panel (a) in Fig. 7 refers to pure superconducting phase and there is no magnetic ordering present. In this situation the current due to hole and electron pockets add up trivially though there is indirect connection between the two current in the sense that the Δ_c is determined by the electron pocket (f -fermions) and Δ_f is determined by hole pocket (c -fermions). As chemical potential is increased, the effective momentum space area determining Δ_c (or

Δ_f) increases or decreases. This results in interdependency of density of states on chemical potential. In the extreme limit when chemical potential is increased beyond a critical value, the superconductivity vanishes and current also vanishes as evident from panel (a) in Fig. 7.

In the panel (b) we plotted the beam splitter current for various values of q for $\mu = 0.2$ and $k_f \delta r = 0$. We see that depending on the values of q , current increases or decreases. We note that a finite q represents co-existence phase with simultaneous presence of magnetic and superconducting orderings in the system. The nature of oscillation is different than the previous case. Here we find a Gaussian-like distribution pointing out that there is an optimal value of the nesting vector for which one obtains maximum beam splitter current. To understand this oscillations we note that in the coexistence phase an eigenvector has the linear combinations of electrons and holes from both the pocket. This quantum entanglement results in specific interference pattern which yields this oscillations, much similar to double-slit diffraction pattern there is central peak with maximum height and subsequent reduced peaks at the two sides of it.

We have shown the density of states for different values of μ (for $q = 0$) in panel (c) and (d) and for q (and $\mu = 0.2$) in panel (e) respectively. In the panel (c), the density of state corresponds to pure magnetic phase while panel (d) corresponds to a pure superconducting phase. The panel (e) corresponds to a coexistence phase. For the pure magnetic phase as in panel (c) the density of states are expected to be peaked around $m + \mu$ for excitation at hole pocket and around $m - \mu$ for electron pocket where m is the magnetic order parameter. This is due to the reason that the modified chemical potential after meanfield approximation are $m \pm \mu$ for electron and hole pocket respectively. For $\mu = 0.05$, our phase diagram in Fig. 4 yields $m \approx 0.6$ and we obtain the peak of density of states around 0.6. As we increase the value of μ , depending on the resulting magnetic order the two peaks occur at approximately $m \pm \mu$.

For the pure superconducting phase the density of states are plotted in panel (d) Fig. 7. We note that for a normal one pocket BCS superconductor the density of state is given by $D_s(E) = \frac{D_n(E_f)E}{\sqrt{E^2 - \Delta^2}}$ where Δ is the superconducting gap and $D_n(E_f)$ is the normal state density of states at $E = E_f$. The density of state shows a divergence at $E = \Delta$ which is due to the sum rule $D_s(E_s)dE_s = D_n(E_n)E_n$ where D_s and D_n are the density of states in superconducting and normal state respectively. E_s and E_n are corresponding energies in the two phases. One can check that for $\mu_c = \mu_f = 0 = m$, the eigenenergies of the two kind of excitations become identical (with $B_k = 0, \Delta_c = -\Delta_f = 0.4$) and density of states shows a divergence at $E = 0.4$. In the presence of finite doping $\mu_{c/f} \neq 0$, this single peak separates into two peaks as evident in panel D, Fig. 7. For finite q , one gets coexistence phase where superconductivity

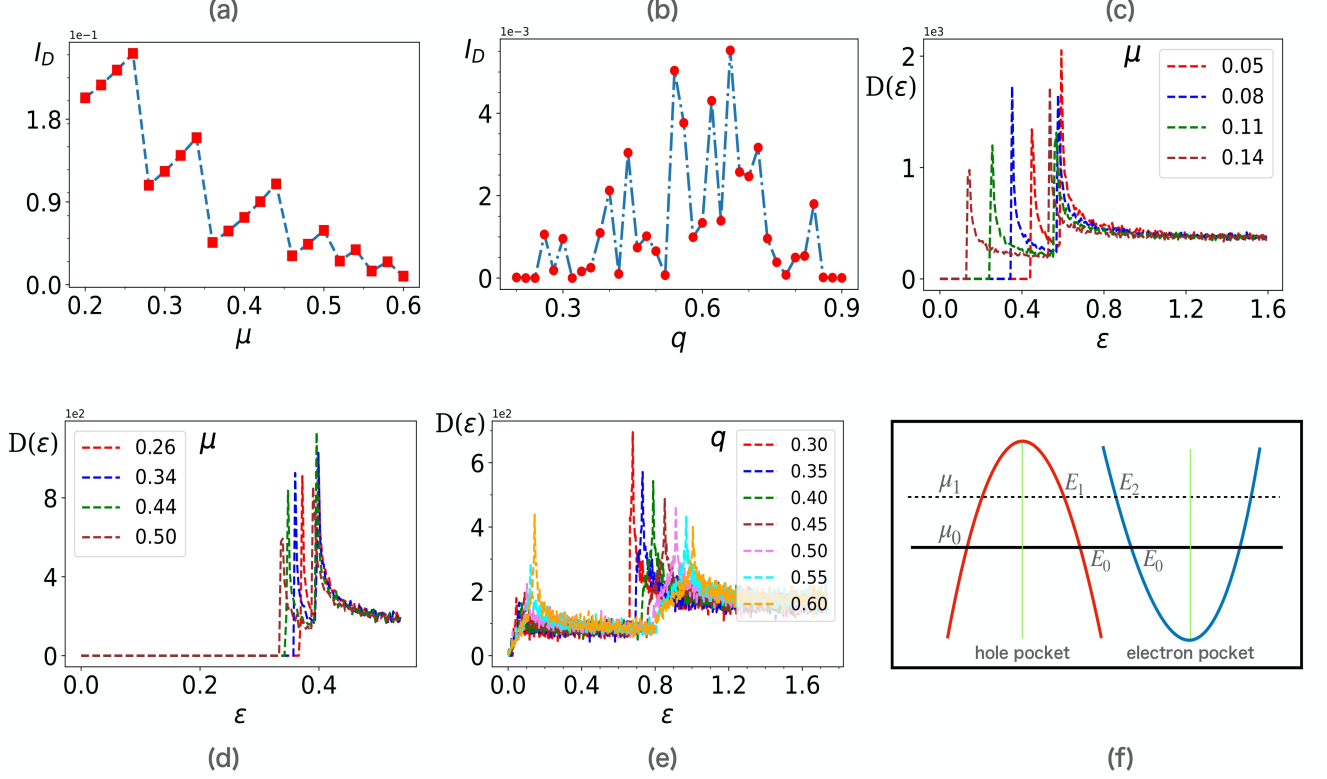


FIG. 7. In the panel (a) beam splitter current is plotted for different dopings for $\mathbf{q}=0$ at $k_f\delta r = 0$. In the panel (b) beam splitter current is plotted against q for $\mu = 0$ and $k_f\delta r = 0$. In both the cases oscillations are observed. In the panel (c) and (d) we plot density of states for representative values of chemical potential (μ) for $q = 0$. Note that according to Fig. 3 panel (c) corresponds to a purely magnetic phase. In the panel (e) we plot density of states for various values of q at $\mu = 0.2$. In panel (f), the effect of electron doping is pictorially shown.

tivity and magnetic ordering both exist. Such coexistence implies that the effective density of states contributing to superconductivity decreases as the sum rule $D_s(E_s)dE_s = D_n(E_n)E_n$ no longer holds. Hence we expect a decrease of current as evident from Fig. 7, the current is two order of magnitude less than the current found in only superconducting phase. The presence of magnetic ordering along with superconductivity causes broadening of the density of states peaks as shown in panel (e) in Fig. 7. In panel (e), Fig. 7 we have taken $\mu = 0.2$ and values of \mathbf{q} varies from 0.3 to 0.6. From panel (b), Fig. 4 we find that for these values of \mathbf{q} values of m ranges increases from 0.2 to 0.4 and the magnitude of Δ_c and Δ_f remain close to 0.4.

V. BEAM CURRENT THROUGH THE SAME DOTS \mathcal{I}_2

Till now we have discussed the scenario where only one of the two electrons(or holes) from the electron (or hole) pocket is collected at either dot and the second electron (or hole) is collected at remaining dot. The current generated from this process is the entangled beam-splitter

current which is matter of interest to us. However the alternative process such as tunneling of two electrons (or holes) via same dot is a real possibility which yields a contribution to current itself. There are two processes in which electron participating in the Cooper pair can tunnel via same dot. Case (I): First one electron(or hole) tunnels from the superconductor to dot-A let's say, and then following it the second electron(or hole) also tunnel to the same dot, as a result there are two electrons (or holes) at the same dot which costs an additional Coulomb repulsion energy of U . Thus this virtual state is suppressed by a factor $1/U$. Finally the two electrons(holes) leave the dot and tunnel to the lead. Case (II): In the other process one electron (or hole) tunnels to say dot-A and then subsequently leaves the dot and tunnels further to lead-A, leaving an excitation on superconductor that costs additional energy Δ before finally the second electron tunnels to the lead-A via dot-A. The current taking into account these two processes can be written as,

$$\mathcal{I}_2 = \frac{2e\gamma_s^2\gamma}{\pi^2\nu_s^2}\mathcal{I}_S, \quad \mathcal{I}_S = \left(\sum_k \mathcal{A}'_k - \mathcal{A}''_k\right)^2 \quad (20)$$

$\gamma_s = 2\pi\nu_s|T_{DS}|^2$ with ν_s is the density of states of the superconductor. $\gamma = \gamma_1 + \gamma_2$ with $\gamma_l = 2\pi\nu_l|T_{DL}|^2$ with ν_l being the density of states at lead 'l'. The expression for \mathcal{A}'_k and \mathcal{A}''_k are given below.

$$\mathcal{A}'_k = \frac{u_{1,k}^c u_{2,k}^c}{E_{1,k}^2} + \frac{u_{1,k}^f u_{2,k}^f}{E_{1,k}^2} + \frac{u_{3,k}^c u_{4,k}^c}{E_{2,k}^2} + \frac{u_{3,k}^f u_{4,k}^f}{E_{2,k}^2} \quad (21)$$

$$\mathcal{A}''_k = \frac{u_{1,\tilde{k}}^c u_{2,\tilde{k}}^c}{E_{1,k}^2} + \frac{u_{1,\tilde{k}}^f u_{2,\tilde{k}}^f}{E_{1,k}^2} + \frac{u_{3,\tilde{k}}^c u_{4,\tilde{k}}^c}{E_{2,k}^2} + \frac{u_{3,\tilde{k}}^f u_{4,\tilde{k}}^f}{E_{2,k}^2} \quad (22)$$

In the above $\tilde{k} = -k$ and expressions for $E_{i,k}$, $u_{i,k}^c$, $u_{i,k}^f$ and $u_{i,\tilde{k}}^c$, $u_{i,\tilde{k}}^f$ are given in the Appendix C. Now in the \mathcal{I}_S as given in Eq. 20, there are two contributions for above mentioned processes which would add up. For detailed calculation of current we request the reader to look into the Appendix-A. To have a comparison between the current as given in Eq. 18 and in Eq. 20, we estimate the ratio between the two. It is straightforward to obtain,

$$\frac{\mathcal{I}_1}{\mathcal{I}_2} = \frac{\mathcal{I}_D}{2\gamma^2 \mathcal{I}_S} \quad (23)$$

Clearly $\mathcal{I}_D > 2\gamma^2 \mathcal{I}_S$ is the the desired regime where \mathcal{I}_1

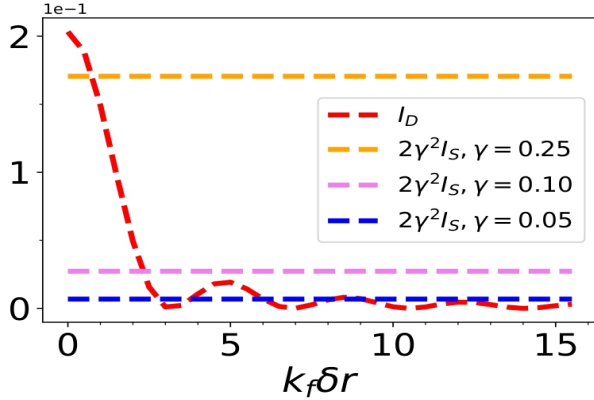


FIG. 8. A comparison of \mathcal{I}_D and \mathcal{I}_S . The oscillating current represents \mathcal{I}_D for $\mu = 0.20$. The constant currents correspond \mathcal{I}_S for various values of γ .

dominates \mathcal{I}_2 . As shown in Fig. 8, for $\gamma = 0.25$ \mathcal{I}_1 is larger than \mathcal{I}_2 for some finite values of $k_f \delta r$. We also observe that a decrease of γ from 0.25 to 0.10 rapidly increases the efficiency of beam-splitter current to larger values of $k_f \delta r$.

Before we conclude and summarize our study, it is imperative to compare the beam-splitter arrangement studied in earlier pioneering work by Daniel loss and collaborators¹⁹ and subsequent extension for graphene based superconductor by Firoz Islam et.al²⁶. Apart from the inherent entangled nature of beam-splitter current, the salient feature of the beam-splitter current for an ideal s-wave BCS supercurrent is characteristic oscillation of current with $k_f \delta r$ which is also present in

graphene based superconductor and also in the present study. Whereas the chemical potential determines the overall magnitude of the beam-splitter current. However there is an important difference found on the dependency of magnitude of beam-splitter current on chemical potential for normal BCS superconductor (and graphene based superconductor) with the iron-pnictide superconductor considered here. The beam-splitter current monotonically decreases as the chemical potential is decreased for ordinary BCS superconductor and graphene based superconductor. But for iron-pnictide system the dependence of overall magnitude of current is non-monotonous with the chemical potential. The reason is the quasi-particle contributing to the beamsplitter current originates from a single fermi-pocket in case of BCS superconductor and graphene based superconductor and thus changing chemical potential has monotonous dependency on the current. However for iron-pnictide the contribution to the beam-splitter current comes from quasi-particles originating from hole and electron pockets separated by a momenta Q . The change of chemical potential effects the size of the electron and hole pocket in opposite way, i.e if electron pocket size is decreased, hole pocket size is increased. Due to the interdependency of beam-splitter current on both the pockets non-trivially, the current varies non-monotonously with the change on chemical potential. Apart from this important difference there are some other significant differences between iron-pnictide superconductor and graphene based superconductor. First of all in graphene the mechanism of superconductivity is not yet established and for this reason proximity based superconductor is assumed. The proximity induced superconductor considered earlier included both s-wave and p-wave superconductor ordering defined as $\Delta_0 = \langle \alpha_{i\uparrow} \alpha_{i\downarrow} \rangle = \langle \beta_{i\uparrow} \beta_{i\downarrow} \rangle$ and $\Delta_1 \sim \langle \alpha_{i\uparrow} \beta_{j\downarrow} - \alpha_{i\downarrow} \beta_{j\uparrow} \rangle$. Here α and β denote the two sublattices in honeycomb lattice. The problem finally reduces as two copies of BCS Hamiltonian in terms of c and d operator which are linear combinations of original α and β by $\alpha_{ks} = \frac{1}{\sqrt{2}}(c_{ks} + d_{ks})$, $\beta_{ks} = \frac{1}{\sqrt{2}}e^{-i\phi_k}(c_{ks} - d_{ks})$. The bogoliubov quasi-particle energy in the “c” and “d” channels are given by $E_{k,\nu} = \sqrt{(\xi_k + \nu\mu)^2 + (g_0\Delta + \nu g_1\Delta_1|\gamma_k|)^2}$, where $\nu = \pm$, where $\nu = +$ for c-channel and $\nu = -$ for d-channel. The Bogoliubov quasi-particles in the c-channel are given by $c_{k,\uparrow} = u_{k,+}\gamma_{1k\uparrow} + v_{k,+}\gamma_{1-k\downarrow}^\dagger$, $c_{-k,\downarrow} = u_{k,+}\gamma_{1-k\downarrow} - v_{k,+}\gamma_{1k\uparrow}^\dagger$. The equivalent relations for the d-channels are given by $d_{k,\uparrow} = u_{k,-}\gamma_{2k\uparrow} + v_{k,-}\gamma_{2-k\downarrow}^\dagger$, $d_{-k,\downarrow} = u_{k,-}\gamma_{2-k\downarrow} - v_{k,-}\gamma_{2k\uparrow}^\dagger$. Here $u_{k,\nu} = \frac{1}{\sqrt{2}}(1 + \frac{\xi_k}{E_{k,\nu}})^{1/2}$ and $v_{k,\nu} = \frac{1}{\sqrt{2}}(1 - \frac{\xi_k}{E_{k,\nu}})^{1/2}$. It has been reported that when only Δ_0 is present the beam-splitter current is larger than the case where Δ_0 and Δ_1 are both present. Though for both the cases the physical problem remains two separated copies of BCS Hamiltonian, the total superconducting quasi-particle density changes when the combinations of order parameters are different. This is ev-

ident as the superconducting number density depends on $\sum_{k,\nu} u_{k\nu} v_{k\nu}$ and $u_{k\nu}$ and $v_{k\nu}$ which depends on $E_{k,\nu}$ through Δ_0 and Δ_1 differently. Thus the physics relies on the re-distribution of quasi-particle density in each blocks. The relation between c and d fermion on the Bogoliubov quasiparticles can be readily compared with the Eqn B2 to Eqn B5. It is evident that in the present case the Bogolubov quasi-particles in c and f channels are not decoupled due to the presence of magnetic order parameters. In the graphene based superconductor such couplings are absent. This coupling between the hole and electron pocket which gives rise to magnetic order parameters are the crucial ingredients for the iron-pnictide based beam-splitter studied here. This gives rise to the non-trivial interference pattern between the two bogoliubov quasiparticles coming from hole and electron pockets.

VI. DISCUSSION

To summarize we have proposed a Cooper pair beam splitter arrangement for Iron-pnictide superconductor which is known for hosting Cooper pairs responsible for superconducting property as well as inherent magnetic ordering. The co-existence of these two seemingly non-inclusive order parameters in a given material provides an interesting platform to investigate the consequences in a Cooper pair beam splitter current. We have considered various realistic situations found in actual materials such as zero nesting and finite nesting³⁹, equal and unequal size of hole and electron pockets etc. Most notably our finding indicates that in general the beam splitter current depends non-monotonically on electron μ_c and hole doping μ_f as well as on the magnitude of nesting vector $|\mathbf{q}|$. In all these cases there are a critical values for which the current is maximum. We believe that this fact might be useful in practical application such as switching and quantum gate applications. In the absence of magnetic ordering the beam splitter current is additive due to hole and electron pocket. However in the co-existence phase due to the entanglement between fermions in electron and hole pocket there are quantum interference effect which results in characteristic oscillations of beam splitter current with respect to nesting vector.

It may also be noted that though in the beamsplitter set up we have assumed $|T_{DS}| < |T_{DL}|$ we do not expect any Kondo effect to set in within the quantum dots because initially in the static limit the quantum dots are taken as vacuum state. Also the tunneling of electron from the lead to quantum dots are suppressed by the grand canonical distribution function $\propto \exp(-\Delta\mu/K_B T)$ where $\Delta\mu$ is the bias voltage. Even a negligible amount of tunneling of normal electron from lead to quantum dot are going to be in even numbers due to participation of electrons of either spins. This would also make the total number of electrons on quantum dots to be even

number which works against Kondo effect to be realized. The effect of external pressure may be an useful way to control the nesting vectors as found before⁴⁷. It may be noted that we have done our calculation of beam splitter current at zero temperature for a prototype iron-pnictide superconductor whereas in real material such superconductivity having coexistence of magnetic order and superconducting order happens upto quite large temperature in comparison to conventional BCS superconductor. We leave the question of finite temperature effect of this beam splitter set up for a future study. However given the fact that all the existing studies so far on beam splitter current is at zero temperature BCS like superconductor and the finite temperature stability of Iron-pnictide superconductor for a wide range of temperature, we think that the study done here would be a realizable at higher temperature than a conventional BCS superconductor based beam-splitter set up.

However we note that the magnitude of the Iron-pnictide based beam-splitter current is smaller in the co-existence phase in order of magnitude than the conventional two dimensional BCS superconductor based beam-splitter current. With the recently proposed protocol of measuring current produced by single electron detection^{51,52} one can expect that the current may be measured. However one also needs to consider the signal to noise ratio for such measurement. We think that our present study would motivate for further investigations on other aspects such as effect of ferromagnetic proximity effect^{22,48}, effect of impurity^{22,48} and Bells inequality⁵⁰.

Finally we note that with the recent significant developments in the field of theoretical and experimental topological insulator based superconductor named topological superconductor, the beam splitter arrangement could serve as an unique set up to detect various quantum mechanical aspect of the topological states as well as the superconducting properties. Recently superconductivity at room temperature has been observed in few-layer Stanene which also host a quantum spin hall phase⁵³. How the robustness of the topological states and superconducting state responds due to various perturbations and disorder is an interesting aspect that can be looked at these topological superconductors⁵³⁻⁵⁶. Further we think the presence of inter-valley scattering in Chern insulator based moire superconductor or in twisted bilayer may have characteristic oscillations or interference pattern in the beam-splitter set up arrangement considered here⁵⁷⁻⁶⁰. However the scope of this study remains open in future.

ACKNOWLEDGMENTS

SM thanks Arijit Saha for useful discussions and S P Mandal for hospitality.

Appendix A: Intermediate steps for current calculation

1. Intermediate steps for current \mathcal{I}_1

Here we give detailed steps to arrive at the current expressions given in Eq. 18 and Eq. 20. We first provide detail steps used to evaluate \mathcal{I}_1 , the current when holes (or electrons) reaches different dots. The main step is to evaluate the transition amplitude $\langle f|T|i \rangle$ defined in Sec. III A. We use Eq. 13, Eq. 14 and Eq. 15 to arrive at the following expression,

$$\begin{aligned} \langle f|T|i \rangle &= \langle f|H_{DL} \sum_{n=0}^{\infty} \left(\frac{1}{i\eta - H} H_{DL} \right)^{2n+1} |f' \rangle \\ &\quad \times \langle f' | \frac{1}{i\eta - H_0} H_{SD} \frac{1}{i\eta - H_0} H_{SD} |i \rangle \\ &= A_{D1} \times A_{D2} \end{aligned} \quad (A1)$$

Where A_{D2} and A_{D1} represent the transition amplitude from superconductor to quantum dots and from quantum dots to lead respectively and their expressions are as follows,

$$A_{D1} = \langle f|H_{DL} \sum_{n=0}^{\infty} \left(\frac{1}{i\eta - H} H_{DL} \right)^{2n+1} |f' \rangle \quad (A2)$$

$$A_{D2} = \langle f' | \frac{1}{i\eta - H_0} H_{SD} \frac{1}{i\eta - H_0} H_{SD} |i \rangle \quad (A3)$$

Where $|f \rangle$ and $|f' \rangle$ are given in Eq. 16 and Eq. 17. Here we note that $|i \rangle$ denotes the combined vacuum state for γ_c, γ_f quasi-particles in superconductor, d -electrons at dots and the a -electrons at lead. The evaluation of A_{D1} and A_{D2} is given in detail below. For simplicity, in the below, we use T' and T'' (as defined in Eqs. 14,15) and

proceed. Then Eq. A16 yields,

$$\begin{aligned} \langle f|T'|f' \rangle &= \frac{1}{2} \langle i | (a_{2q\downarrow} a_{1p\uparrow} - a_{2q\uparrow} a_{1p\downarrow}) T' \times \\ &\quad (d_{1\uparrow}^+ d_{2\downarrow}^+ - d_{1\downarrow}^+ d_{2\uparrow}^+) |i \rangle \\ &= \frac{1}{2} \langle i | a_{2q\downarrow} a_{1p\uparrow} T' d_{1\uparrow}^+ d_{2\downarrow}^+ |i \rangle \\ &\quad - \underbrace{\langle i | a_{2q\downarrow} a_{1p\uparrow} T' d_{1\downarrow}^+ d_{2\uparrow}^+ |i \rangle}_{=0} \\ &\quad - \underbrace{\langle i | a_{2q\uparrow} a_{1p\downarrow} T' d_{1\uparrow}^+ d_{2\downarrow}^+ |i \rangle}_{=0} \\ &\quad + \langle i | a_{2q\uparrow} a_{1p\downarrow} T' d_{1\downarrow}^+ d_{2\uparrow}^+ |i \rangle \end{aligned} \quad (A4)$$

We note that in the above a -operators denote the fermions at the leads and d -operators denote the fermions at the quantum dots and we have used the spin-singlet states at the lead and dots. Now the underbraced terms vanish because spin flip is happening which is not allowed by the design mechanism of the splitter. Also it is interesting to notice that first and last terms are identical under exchange of spin indices ($\uparrow \rightleftharpoons \downarrow$). All these imply that,

$$\langle f|T'|f' \rangle = \frac{1}{2} 2 \langle i | a_{2q\downarrow} a_{1p\uparrow} T' d_{1\uparrow}^+ d_{2\downarrow}^+ |i \rangle \quad (A5)$$

Similarly for the Andreev process which denotes the tunneling of electrons from superconductor to quantum dots as denoted by Eq. A3,

$$\langle f'|T''|i \rangle = \frac{1}{\sqrt{2}} \langle i | (d_{2\downarrow} d_{1\uparrow} - d_{2\uparrow} d_{1\downarrow}) T'' |i \rangle \quad (A6)$$

Now it may happen that in the process of transport one electron with a particular spin(say up) comes to the dot from the superconductor but an electron with opposite spin(say down) may travel forward from the same dot to the lead, but we don't want that. We want processes like $|SS \rangle \rightarrow |DS \rangle \rightarrow |DD \rangle$ and $|SS \rangle \rightarrow |SD \rangle \rightarrow |DD \rangle$ such that entangled pair of electrons from the superconductor(SS) get transported to dot(DD) and move forward to separate leads, because we avoid spin flipping. Where, $|SD \rangle = \sum_{\phi} \gamma_{k\sigma}^{\phi+} d_{l-\sigma}^+ |i \rangle$. ϕ can take c and f two values due to two species of quasiparticles and γ denotes the Bogoliubov quasiparticles in the superconductor. To proceed further we note few important points for the below calculations; (a) H_{S1D1} selects one electron of the entangled pair to dot 1 and H_{S2D2} selects the other electron of the entangled pair to dot 2. (b) We take $+k$ for \uparrow spin and $-k$ for \downarrow spin without loss of generality. We also note that, in the following, we use the Bogoliubov transformations given in Eqs. B2,B3,B4,B5 and the Fourier transformations, $\Psi_{\sigma}^c(\bar{r}_l) = \sum_k e^{i\bar{k} \cdot \bar{r}_l} c_{k\sigma} = \sum_{-k} e^{-i\bar{k} \cdot \bar{r}_l} c_{-k\sigma}$ and $\Psi_{\sigma}^f(\bar{r}_l) = \sum_k e^{i\bar{k} \cdot \bar{r}_l} f_{k\sigma} = \sum_{-k} e^{-i\bar{k} \cdot \bar{r}_l} f_{-k\sigma}$ which are required while using H_{SD} as given in Eq. 11. It is also to be noted that since we work close to resonance we use $|i\eta - E_k - \epsilon_l| \approx |E_k|$ where E_k and ϵ_l denotes the energy of the Bogoliubov quasiparticle and energy of quantum dot. Now we proceed to simplify $\langle f'|T''|i \rangle$ as follows,

$$\begin{aligned}
\langle f'|T''|i \rangle &= \frac{1}{\sqrt{2}} \langle i|(d_{2\downarrow}d_{1\uparrow} - d_{2\uparrow}d_{1\downarrow}) \frac{1}{(i\eta - H_0)} H_{s_1 D_1} \sum_{k,l,\sigma,\phi=c,f} \gamma_{k\sigma}^{\phi+} d_{l-\sigma}^+ |i \rangle \langle i| d_{l-\sigma} \gamma_{k\sigma}^{\phi} \frac{1}{(i\eta - H_0)} H_{s_2 D_2} |i \rangle \\
&= \frac{1}{\sqrt{2}} \langle i|(d_{2\downarrow}d_{1\uparrow} - d_{2\uparrow}d_{1\downarrow}) \frac{1}{(i\eta - H_0)} [\sum_{l\sigma,\phi=c,f} T_{SD} d_{1\sigma}^+ \psi_{\sigma}^{\phi}(\bar{r}_l) + h.c.] \sum_{k,l,\sigma,\phi=c,f} \gamma_{k\sigma}^{\phi+} d_{l-\sigma}^+ |i \rangle \\
&\quad \langle i| d_{l-\sigma} \gamma_{k\sigma}^{\phi} \frac{1}{(i\eta - H_0)} [\sum_{l\sigma,\phi=c,f} T_{SD} d_{2\sigma}^+ \psi_{\sigma}^{\phi}(\bar{r}_l) + h.c.] |i \rangle \\
&= \frac{1}{\sqrt{2}} [\sum_k \langle i| d_{2\downarrow} d_{1\uparrow} \frac{1}{(i\eta - H_0)} T_{SD} d_{1\uparrow}^+ [c_{k\uparrow} + f_{k\uparrow}] [\gamma_{k\uparrow}^{c+} + \gamma_{k\uparrow}^{f+}] d_{2\downarrow}^+ e^{i\bar{k} \cdot \bar{r}_1} |i \rangle \times \\
&\quad \langle i| d_{2\downarrow} [\gamma_{k\uparrow}^c + \gamma_{k\uparrow}^f] \frac{1}{(i\eta - H_0)} T_{SD} d_{2\downarrow}^+ [c_{-k\downarrow} + f_{-k\downarrow}] e^{-i\bar{k} \cdot \bar{r}_2} |i \rangle] \\
&\quad - \frac{1}{\sqrt{2}} [\sum_k \langle i| d_{2\uparrow} d_{1\downarrow} \frac{1}{(i\eta - H_0)} T_{SD} d_{1\downarrow}^+ [c_{-k\downarrow} + f_{-k\downarrow}] [\gamma_{-k\downarrow}^{c+} + \gamma_{-k\downarrow}^{f+}] d_{2\uparrow}^+ e^{-i\bar{k} \cdot \bar{r}_1} |i \rangle \times \\
&\quad \langle i| d_{2\uparrow} [\gamma_{-k\downarrow}^c + \gamma_{-k\downarrow}^f] \frac{1}{(i\eta - H_0)} T_{SD} d_{2\uparrow}^+ [c_{k\uparrow} + f_{k\uparrow}] e^{i\bar{k} \cdot \bar{r}_2} |i \rangle] \\
&= \frac{1}{\sqrt{2}} [\sum_k \frac{T_{SD}^2}{\epsilon_1 + \epsilon_2 - i\eta} \mathcal{A}_k(\cos \bar{k} \cdot \delta \bar{r})]
\end{aligned} \tag{A7}$$

Note that the $\sin(\bar{k} \cdot \delta \bar{r})$ term associated with imaginary part will go to zero while doing the θ integration in k sum. The factor \mathcal{A}_k is given in Eq. 19 and ϵ_1, ϵ_2 denote the energies at quantum dot 1 and 2 respectively. We have mentioned earlier that there can be two ways of tunneling from superconductor to quantum dots. Both the processes gives identical expressions which results in a multiplicative factor of 2. Incorporating this finally we obtain,

$$\langle f'|T''|i \rangle = \frac{1}{\sqrt{2}} [\sum_k \frac{2T_{SD}^2}{\epsilon_1 + \epsilon_2 - i\eta} \mathcal{A}_k(\cos \bar{k} \cdot \delta \bar{r})] \tag{A8}$$

Now lets calculate the second term as given in Eq. A5 in the below.

$$\langle f'|T'|f' \rangle = \frac{1}{2} 2 \langle i| a_{2q\downarrow} a_{1p\uparrow} T' d_{1\uparrow}^+ d_{2\downarrow}^+ |i \rangle \tag{A9}$$

The above process signify tunneling from quantum dots to the leads which are symbolically denoted as $|DD \rangle = |LD \rangle = |DD \rangle$ and $|DD \rangle = |DL \rangle = |DD \rangle$. Here $|LD \rangle$ (or $|DL \rangle$) denotes the state after one electron reaches to first (or second) lead via respective quantum dots. In the subsequent steps we denote the lead states $|LL \rangle$ as $|pq \rangle$ for notational conveniences. From the detail expressions of $\langle f'|T'|f' \rangle$ from Eq. A16 we note that various intermediate steps are to be inserted appropriately as allowed by Wick's theorem and orthogonality condition. Considering all such possible processes we can

write down,

$$\begin{aligned}
\langle f'|T'|f' \rangle &= \langle pq|T'|DD \rangle \\
&= [\langle pq|H_{D_1 L_1}|Dq \rangle \\
&\quad \times \langle Dq|(\sum_{n=0}^{\infty} (\frac{1}{i\eta - H_0} H_{D_1 L_1})^{2n}|Dq \rangle \\
&\quad \times \langle Dq|\frac{1}{i\eta - H_0} H_{D_2 L_2}|DD \rangle + \\
&\quad \langle pq|H_{D_2 L_2}|pD \rangle \\
&\quad \times \langle pD|\sum_{n=0}^{\infty} (\frac{1}{i\eta - H_0} H_{D_2 L_2})^{2n}|pD \rangle \\
&\quad \times \langle pD|\frac{1}{i\eta - H_0} H_{D_1 L_1}|DD \rangle] \\
&\quad \times \langle DD|\sum_{m=0}^{\infty} (\frac{1}{i\eta - H_0} H_{DL})^{2m}|DD \rangle
\end{aligned} \tag{A10}$$

Just calculating like before it is straightforward to have¹⁹,

$$\begin{aligned}
\langle DD|\sum_{m=0}^{\infty} (\frac{1}{i\eta - H_0} H_{DL})^{2m}|DD \rangle &= \tag{A11} \\
&\frac{1}{1 - \langle DD|(\frac{1}{i\eta - H_0} H_{DL})^2|DD \rangle}
\end{aligned}$$

where $\langle DD|(\frac{1}{i\eta - H_0} H_{DL})^2|DD \rangle = \frac{\Sigma}{i\eta - \epsilon_1 - \epsilon_2}$, $\Sigma = |T_{DL}|^2 \sum_{lk} (i\eta - \epsilon_l - \epsilon_k)^{-1}$. In the presence of a Fermi sea in the leads we introduce a cutoff in the sum in Σ at the fermi level given by $\epsilon_k \sim -\Delta\mu$ and at the edge of the conduction band given by ϵ_c . Then one obtains $\Sigma = \gamma_l \ln(\epsilon_c/\Delta\mu) - i\gamma/2$. Now we note that logarithmic renormalization of the self energy is small i.e., \sim

$\gamma_l \ln(\epsilon_c/\Delta\mu) < \Delta\mu$ and for this we neglect this in the following. Here we have used $\gamma_l = 2\pi\nu_l|T_{DL}|^2$, $\gamma = \gamma_1 + \gamma_2$, where ν_l is the DOS at the chemical potential μ_l . All these yields the following simplification,

$$\langle DD | \sum_{m=0}^{\infty} \left(\frac{1}{i\eta - H_0} H_{DL} \right)^{2m} | DD \rangle = \frac{\epsilon_1 + \epsilon_2 - i\eta}{\epsilon_1 + \epsilon_2 - i\gamma/2} \quad (\text{A12})$$

Similarly,

$$\langle pD | \sum_{n=0}^{\infty} \left(\frac{1}{i\eta - H_0} H_{D_2L_2} \right)^{2n} | pD \rangle = \frac{\epsilon_p + \epsilon_2 - i\eta}{\epsilon_p + \epsilon_2 - i\gamma_2/2} \quad (\text{A13})$$

and

$$\langle Dq | \sum_{n=0}^{\infty} \left(\frac{1}{i\eta - H_0} H_{D_1L_1} \right)^{2n} | Dq \rangle = \frac{\epsilon_q + \epsilon_1 - i\eta}{\epsilon_q + \epsilon_1 - i\gamma_1/2} \quad (\text{A14})$$

Inserting Eqs. A12, A13 and A14 in Eq. A10 we obtain,

$$\begin{aligned} \langle pq | T' | DD \rangle &= \left[\frac{|T_{DL}|^2}{(i\eta - \epsilon_1 - \epsilon_q)} \times \frac{(\epsilon_1 + \epsilon_q - i\eta)}{(\epsilon_1 + \epsilon_q - i\frac{\gamma_1}{2})} \right] \\ &\quad + \frac{|T_{DL}|^2}{(i\eta - \epsilon_2 - \epsilon_p)} \times \frac{(\epsilon_2 + \epsilon_p - i\eta)}{(\epsilon_2 + \epsilon_p - i\frac{\gamma_2}{2})} \\ &\quad \times \frac{(\epsilon_1 + \epsilon_2 - i\eta)}{(\epsilon_1 + \epsilon_2 - i\frac{\gamma}{2})} \\ &= - \frac{|T_{DL}|^2 (\epsilon_1 + \epsilon_2 - i\eta)}{(\epsilon_1 + \epsilon_q - i\frac{\gamma_1}{2})(\epsilon_2 + \epsilon_p - i\frac{\gamma_2}{2})} \end{aligned} \quad (\text{A15})$$

Thus the final expression for AD_1 and AD_2 as obtained are given below,

$$A_{D1} = - \frac{|T_{DL}|^2 (\epsilon_1 + \epsilon_2 - i\eta)}{(\epsilon_1 + \epsilon_q - i\gamma_1/2)(\epsilon_2 + \epsilon_p - i\gamma_2/2)} \quad (\text{A16})$$

$$A_{D2} = \frac{1}{\sqrt{2}} \left[\sum_k \frac{2|T_{SD}|^2}{\epsilon_1 + \epsilon_2 - i\eta} \mathcal{A}_k(\cos \bar{k} \cdot \delta \bar{r}) \right] \quad (\text{A17})$$

In the above ϵ_1 and ϵ_2 represent the energy of quantum dot 1 and dot 2 respectively. The factor containing η cancels due to contribution from A_{D1} and A_{D2} . Also we note that in obtaining AD_1 , we have removed the η factors in the denominators as they are replaced by γ_l at the end. Note that the energy of the Bogoliubov quasiparticle $\mathcal{E}_{kq\pm}$ does not appear in the above two expressions as the initial state $|i\rangle$ is taken as vacuum of Bogoliubov quasiparticle. The full expression of \mathcal{A}_k (as obtained in A7) is given below.

$$\begin{aligned} \mathcal{A}_k &= \frac{u_{1,k}^c u_{2,k}^c - u_{1,-k}^c u_{2,-k}^c}{\mathcal{E}_{kq+}} + \frac{u_{1,k}^f u_{2,k}^f - u_{1,-k}^f u_{2,-k}^f}{\mathcal{E}_{kq+}} \\ &\quad + \frac{u_{3,k}^c u_{4,k}^c - u_{3,-k}^c u_{4,-k}^c}{\mathcal{E}_{kq-}} + \frac{u_{3,k}^f u_{4,k}^f - u_{3,-k}^f u_{4,-k}^f}{\mathcal{E}_{kq-}} \end{aligned} \quad (\text{A18})$$

Using Eq. A16 and Eq. A17 we arrive at the current expression given in Eq. 18.

2. Intermediate steps for current \mathcal{I}_2

Now we outline the intermediate steps to arrive at the expression for \mathcal{I}_2 . Similar to Eq. A1 we find the following expression for the transition amplitude $\langle f | T | i \rangle$,

$$\begin{aligned} \langle f | T | i \rangle &= \sum_{p''\sigma} \langle f | H_{DL} \sum_{n=0}^{\infty} \left(\frac{1}{i\eta - H_0} H_{DL} \right)^{2n} | f' \rangle \times \\ &\quad \langle f' | \frac{1}{i\eta - H_0} H_A \frac{1}{i\eta - H_0} H_B \frac{1}{i\eta - H_0} H_C | i \rangle \\ &= \sum_{p''\sigma} A_{S1\sigma} \times A_{S2\sigma} \end{aligned} \quad (\text{A19})$$

$$(\text{A20})$$

Here $A_{S1\sigma}$ and $A_{S2\sigma}$ are given below,

$$A_{S1\sigma} = \langle f | H_{DL} \sum_{n=0}^{\infty} \left(\frac{1}{i\eta - H_0} H_{DL} \right)^{2n} | f' \rangle \quad (\text{A21})$$

$$A_{S2\sigma} = \langle f' | \frac{1}{i\eta - H_0} H_A \frac{1}{i\eta - H_0} H_B \frac{1}{i\eta - H_0} H_C | i \rangle \quad (\text{A22})$$

where $|f\rangle = (1/\sqrt{2})(a_{p\uparrow}^\dagger a_{p'\downarrow}^\dagger - a_{p\downarrow}^\dagger a_{p'\uparrow}^\dagger)|i\rangle$ is the singlet final state and $|f'\rangle = |Dp''\sigma\rangle = d_{-\sigma}^\dagger a_{p''\sigma}^\dagger |i\rangle$ is the intermediate state which tells that one electron is in the dot while the other has tunneled to lead. The subscripts A, B, C used above in H depends a combination of different tunneling Hamiltonian. In the first case (case (I)) A, B, C denotes $SD, DL \& SD$ respectively. For the second case (case (II)) A, B, C denote $DL, SD, \& SD$ respectively. For case (I), as evident, one electron from superconductor enters into a quantum dot (by the action of T_{SD}), the same electron then moves to lead by T_{DL} and finally the second electron arrives at quantum dot by T_{SD} . For case (II), it is evident that both the electrons arrive at the same dot by repeated action of T_{SD} costing an interaction energy U . Utilizing the above facts we can simplify as before to obtain AD_1 and AD_2 in Eq. A7 and A10. A straightforward procedure yields the following the expressions for $A_{S\sigma}$,

$$A_{S1\sigma} = r_\sigma \frac{T_{DL}}{\sqrt{2}} \frac{\epsilon_l + \epsilon_p'' - i\eta}{\epsilon_l + \epsilon_p'' - i\gamma_l/2} (\delta_{p''p'} + \delta_{p''p}) \quad (\text{A23})$$

$$A_{S2\sigma} = \frac{T_{DL} T_{SD}^2}{\epsilon_l + \epsilon_{p''} - i\eta} \mathcal{B}_{k\sigma} \quad (\text{A24})$$

In the above σ refers spin indices and could be \uparrow or \downarrow and we have $r_\uparrow = -1$, $r_\downarrow = 1$. The expressions for $\mathcal{B}_{k\uparrow}$ and $\mathcal{B}_{k\downarrow}$ are obtained as follows,

$$\mathcal{B}_{k\uparrow} = \frac{u_{1,k}^c u_{2,k}^c + u_{1,k}^f u_{2,k}^f}{\mathcal{E}_{kq+}^2} + \frac{u_{3,k}^c u_{4,k}^c + u_{3,k}^f u_{4,k}^f}{\mathcal{E}_{kq-}^2} \quad (\text{A25})$$

$$\mathcal{B}_{k\downarrow} = \frac{u_{1,\tilde{k}}^c u_{2,\tilde{k}}^c + u_{1,\tilde{k}}^f u_{2,\tilde{k}}^f}{\mathcal{E}_{kq+}^2} + \frac{u_{3,\tilde{k}}^c u_{4,\tilde{k}}^c + u_{3,\tilde{k}}^f u_{4,\tilde{k}}^f}{\mathcal{E}_{kq-}^2} \quad (\text{A26})$$

In the last equation we have used $\tilde{k} = -k$. After some algebra we arrive at the final current expressions as given in Eq. 18 and Eq. 20. Now let's calculate I_1/I_2 for getting an idea about their relative strength. Firstly for Breit-Wigner resonance we have $\epsilon_1 = -\epsilon_2$, which further reduces $\mathcal{I}_1 = \frac{e\gamma_s^2}{\pi^2\nu_s^2\gamma}\mathcal{I}_D$. using this we get,

$$\frac{\mathcal{I}_1}{\mathcal{I}_2} = \frac{\mathcal{I}_D}{2\gamma^2\mathcal{I}_S} \quad (\text{A27})$$

Clearly $1/\gamma^2 > \mathcal{I}_S/\mathcal{I}_D$ is the the desired regime where \mathcal{I}_1 dominates \mathcal{I}_2 . We notice that in \mathcal{I}_S expression there is an additional supression of $\mathcal{E}_{kq\pm}$ compared to \mathcal{I}_D which suggests that \mathcal{I}_2 is suppressed compared to \mathcal{I}_1 .

Appendix B: Appendixes-B

After diagonalisation and filling the negative energy states we obtain the following ground state energy, The ground state energy of the superconductor is given below,

$$E_{min} = -\sum_{kk's} (\mathcal{E}_{kq+} + \mathcal{E}_{kq-}) - 2\frac{\Delta_c\Delta_f}{V_{SC}} + 2\frac{m^2}{V_{SD}} \quad (\text{B1})$$

Where $\mathcal{E}_{kq\pm} = \frac{1}{\sqrt{2}}\sqrt{(\mathcal{P}_k \pm \sqrt{\mathcal{Q}_k})}$. The function $\mathcal{P}_k = \Delta_c^2 + \Delta_f^2 + \epsilon_c^2(k) + \epsilon_f^2(k) + 2m^2$ and $\mathcal{Q}_k = (\Delta_c^2 - \Delta_f^2 + \epsilon_c^2(k) - \epsilon_f^2(k))^2 + 4m^2((\Delta_c - \Delta_f)^2 + (\epsilon_c(k) + \epsilon_f(k))^2)$. The Bogoliubov transformations for the present case can be written as follows.

$$c_{k\sigma} = u_{1k}^c \gamma_{kq\sigma}^c + u_{1\tilde{k}}^c \gamma_{k\tilde{\sigma}}^{c\dagger} + u_{1k'}^f \gamma_{k'\sigma}^f + u_{1\tilde{k}'}^f \gamma_{k'\tilde{\sigma}}^{f\dagger} \quad (\text{B2})$$

$$c_{\tilde{k}\tilde{\sigma}}^\dagger = u_{2k}^c \gamma_{k\sigma}^c + u_{2\tilde{k}}^c \gamma_{k\tilde{\sigma}}^{c\dagger} + u_{2k'}^f \gamma_{k'\sigma}^f + u_{2\tilde{k}'}^f \gamma_{k'\tilde{\sigma}}^{f\dagger} \quad (\text{B3})$$

$$f_{k'\sigma} = u_{3k}^c \gamma_{k\sigma}^c + u_{3\tilde{k}}^c \gamma_{k\tilde{\sigma}}^{c\dagger} + u_{3k'}^f \gamma_{k'\sigma}^f + u_{3\tilde{k}'}^f \gamma_{k'\tilde{\sigma}}^{f\dagger} \quad (\text{B4})$$

$$f_{\tilde{k}'\tilde{\sigma}}^\dagger = u_{4k}^c \gamma_{k\sigma}^c + u_{4\tilde{k}}^c \gamma_{k\tilde{\sigma}}^{c\dagger} + u_{4k'}^f \gamma_{k'\sigma}^f + u_{4\tilde{k}'}^f \gamma_{k'\tilde{\sigma}}^{f\dagger} \quad (\text{B5})$$

In the above we have used ($\tilde{k} = -k$, $\tilde{\sigma} = -\sigma$). Also $k' = k + q$, $\tilde{k}' = -k + q$; q is the ordering momentum and u 's are the elements of the eigen vectors of

the Hamiltonian given in Eq. 12. Considering 'c' or 'f' to be generally denoted by 'p' and $+k$ or $-k$ denoted by 'z', the expressions for all the u 's can be written as $u_{iz}^p = \frac{a_{iz}^p}{\sqrt{\sum_{zp}(a_{iz}^p)^2}}$. Henceforth for simplification we remove the explicit mention of momentum indices in all the variables and define $\zeta = (\epsilon_f - \epsilon_c)/2$, $\delta = (\epsilon_f + \epsilon_c)/2$, $\Delta_{\pm} = (\Delta_c \pm \Delta_f)/2$ and $\alpha = \sqrt{(\Delta_+ \Delta_- - \delta\zeta)^2 + m^2(\Delta_-^2 + \delta^2)}$, $\Omega_{\pm} = \Delta_+ \delta + \Delta_- (\zeta \pm E_1)$ and $\Omega'_{\pm} = \Delta_+ \delta + \Delta_- (\zeta \pm E_2)$ with $E_{1,2} = \sqrt{A \pm \sqrt{B}}$. Below we provide details expressions of a_i 's.

$$a_{1(2),k}^c = \frac{(m^2\delta + (\delta + \zeta + (-)E_1)(\lambda_1 - \alpha))}{m\Omega_{+(-)}}, \quad (\text{B6})$$

$$a_{3(4),k}^c = \frac{(m^2\delta + (\delta + \zeta + (-)E_2)(\lambda_1 + \alpha))}{m\Omega'_{+(-)}}, \quad (\text{B7})$$

$$a_{1(2),-k}^c = \frac{(\Delta_+(\Delta_-^2 + \delta\zeta - \alpha) - \Delta_-(\lambda_2 - \alpha))}{m\Omega_{+(-)}} \quad (\text{B8})$$

$$a_{3(4),-k}^c = \frac{(\Delta_+(\Delta_-^2 + \delta\zeta + \alpha) - \Delta_-(\lambda_2 + \alpha))}{m\Omega'_{+(-)}} \quad (\text{B9})$$

In the above $\lambda_1 = -\Delta_+\Delta_- + \delta\zeta$, $\lambda_2 = \Delta_+^2 + \delta\zeta + m^2$. Expressions for $a_{i,k}^f$ are comparatively simpler and given by,

$$a_{1(2),k}^f = \frac{(\Delta_-^2 + \delta^2 - \alpha + (-)\delta E_1)}{\Omega_{+(-)}} \quad (\text{B10})$$

$$a_{3(4),k}^f = \frac{(\Delta_-^2 + \delta^2 + \alpha + (-)\delta E_2)}{\Omega'_{+(-)}} \quad (\text{B11})$$

$$a_{i,-k}^f = 1, \quad i = 1, 2, 3, 4 \quad (\text{B12})$$

One can check that the above expressions get simplified for $m = 0$ case and we only mention the non-zero elements below.

$$a_{3(4),k}^c = \frac{-\delta - \zeta - (+)\sqrt{(\Delta_+ - \Delta_-)^2 + (\delta + \zeta)^2}}{\Delta_- - \Delta_+} \quad (\text{B13})$$

$$a_{1(2),k}^f = \frac{\delta - \zeta + (-)\sqrt{(\Delta_+ + \Delta_-)^2 + (\delta - \zeta)^2}}{\Delta_- + \Delta_+} \quad (\text{B14})$$

$$a_{3,-k}^c = a_{4,-k}^c = a_{1,-k}^f = a_{2,-k}^f = 1 \quad (\text{B15})$$

* abhisek.b@iopb.res.in

† saptarshi@iopb.res.in

¹ J. J. Sakurai, Jim Napolitano, Modern Quantum Mechanics, Cambridge University Press, 3rd Edition(2020)

² Michael A. Neilson and Isacc L. Chuang Quantum Computations and Quantum Informations, Cambridge University Press (2003).

³ David P. DiVincenzo, Fortschr. Phys. **48**, (2000) 9-11, 771-

- 783
- ⁴ Ivan Djordjevic, Quantum Information Processing and Quantum Error Correction, 2012
 - ⁵ T. Bækgaard, L. B. Kristensen, N. J. S. Loft, C. K. Andersen, D. Petrosyan & N. T. Zinner, Scientific Reports volume 9, Article number: 13389 (2019)
 - ⁶ Ashley Montanaro, npj Quantum Information volume 2, Article number: 15023 (2016)
 - ⁷ Walter Pötz Ulrich Hohenester Jaroslav Fabian, Quantum Coherence From Quarks to Solids, Springer
 - ⁸ T. van der Sar, Z. H. Wang, M. S. Blok, H. Bernien, T. H. Taminiau, D. M. Toyli, D. A. Lidar, D. D. Awschalom, R. Hanson & V. V. Dobrovitski, Nature volume **484**, pages 82–86 (2012)
 - ⁹ Tinkham, Michael (1996). Introduction to Superconductivity. Dover Publications.
 - ¹⁰ Yi Zhou, Kazushi Kanoda, and Tai-Kai Ng, Rev. Mod. Phys. **89**, 025003 (2017)
 - ¹¹ Lucile Savary and Leon Balents, 2017 Rep. Prog. Phys. **80**, 016502
 - ¹² G Baskaran, Z Zou and P W Anderson, Sol. State Commun. **63**, 973 (1987)
 - ¹³ A. Einstein, B. Podolsky, and N. Rosen, Phys. Rev. **47**, 777 (1935)
 - ¹⁴ J.S. Bell, Speakable and unspeakable in quantum mechanics, Cambridge University Press, Cambridge, 1987
 - ¹⁵ A. Peres, Quantum theory: Concepts and methods, Kluwer, Dordrecht, 1993.
 - ¹⁶ Bei Zeng, Xie Chen, Duan-Lu Zhou, Xiao-Gang Wen, Quantum Information Meets Quantum Matter – From Quantum Entanglement to Topological Phase in Many-Body Systems, Springer, 2019 (Book). arXiv:1508.02595
 - ¹⁷ Nicolas Laflorencie, Physics Report Volume 643, 1–59 (2016)
 - ¹⁸ Andreas Osterloh, arXiv:0810.1240
 - ¹⁹ Patrik Recher, Eugene V. Sukhorukov, and Daniel Loss, Phys. Rev. B. **63**, 165314 (2001)
 - ²⁰ L. Hofstetter, S. Csonka, J. Nygard and C. Schönenberger, Nature, Vol 461, 08432, 2009
 - ²¹ L. G. Herrmann, F. Portier, P. Roche, A. L. Yeyati, T. Kontos, and C. Strunk, Phys. Rev. Lett. **104**, 026801 (2010).
 - ²² P. Burset, W. J. Herrera, and A. Levy Yeyati, Phys. Rev. B **84**, 115448 (2011)
 - ²³ Koji Sato, and Yaroslav Tserkovnyak, Phys. Rev. B **90**, 045419, 2014
 - ²⁴ Mattia Mantovani, Wolfgang Belzig, Gianluca Rastelli, and Robert Hussein, Phys. Rev. Research **1**, 033098 (2019)
 - ²⁵ Constantinos Valagiannopoulos, Phys. Rev. Applied **12**, 054042 (2019)
 - ²⁶ SK Firoz Islam and Arijit Saha, Phys. Rev. B. **96**, 125406 (2017)
 - ²⁷ Michael R. Norman, The Challenge of Unconventional Superconductivity, 8 APRIL 2011 VOL 332 SCIENCE
 - ²⁸ Yunkyu Bang and G R Stewart 2017 J. Phys.: Condens. Matter **29** 123003
 - ²⁹ I. I. Mazin, D. J. Singh, M. D. Johannes, and M. H. Du, Phys. Rev. Lett. **101**, 057003 (2008)
 - ³⁰ M.K. Wu et al. Phys. Rev. Lett., 58 (9) (1987), p. 908
 - ³¹ Hideo Hosono, Akiyasu Yamamoto, Hidenori Hiramatsu, Yanwei Ma, Materials Today, Volume 21, Number 3, April 2018
 - ³² Hai-Hu Wen and Shiliang Li, Annu. Rev. Condens. Matter Phys. 2011. 2:121–40
 - ³³ G. R. Stewart, REVIEWS OF MODERN PHYSICS, VOLUME 83, OCTOBER–DECEMBER 2011
 - ³⁴ Qimiao Si, Rong Yu, Elihu Abrahams, Nature Rev. Mater. **1**, 16017 (2016). arXiv:1604.03566
 - ³⁵ F. Steglich, Physica C: Superconductivity and its Applications, Volumes 460–462, Part 1, 2007, Pages 7–12
 - ³⁶ D. J. Singh, Acta Physica Polonica A, **121**, 2012
 - ³⁷ A. Subedi, L. Zhang, D. J. Singh, and M. H. Du, Phys. Rev. B **78**, 134514 (2008)
 - ³⁸ A. V. Chubukov, Physica C **469**, 640, 2009
 - ³⁹ A. V. Chubukov, V. Efremov and I. Eremin, Phys. Rev. B **78**, 134512 (2008)
 - ⁴⁰ A. B. Vorontsov, M. G. Vavilov and A. V. Chubukov, Phys. Rev. B **81**, 174538 (2010)
 - ⁴¹ M A N Araujo, M Cardoso and P D Sacramento, New Journal of Physics **11** (2009) 113008
 - ⁴² Yunkyu Bang and Han-Yong Choi, Phys. Rev. B **78**, 134523 (2008)
 - ⁴³ Xiang Hu, C. S. Ting, Jian-Xin Zhu, Phys. Rev. B **80**, 014523 (2009)
 - ⁴⁴ Hong-Min Jiang, Jian-Xin Li and Z. D. Wang, Phys. Rev. B **80**, 134505 (2009)
 - ⁴⁵ M. Sumetskiĭ, Phys. Rev. B **48**, 4586 (1993)
 - ⁴⁶ E. Merzbacher, Quantum Mechanics, 3rd ed. (Wiley, New York, 1998), Chap. 20
 - ⁴⁷ Vladimir Cvetkovic and Zlatko Tesanovic, Phys. Rev. B **80**, 024512 (2009)
 - ⁴⁸ L. Hofstetter, A. Geresdi, M. Aagesen, J. Nygard, C. Schönenberger, and S. Csonka, Phys. Rev. Lett. **104**, 246804 (2010)
 - ⁴⁹ J. Rech, D. Chevallier, T. Jonckheere, and T. Martin, Phys. Rev. B **85**, 035419 (2012)
 - ⁵⁰ P. Samuelsson, E. V. Sukhorukov, and M. Büttiker, Phys. Rev. Lett. **91**, 157002 (2003)
 - ⁵¹ Jonas Bylander, Tim Duty and Per Delsing, Nature volume **434**, pages 361–364 (2005)
 - ⁵² Toshimasa Fujisawa, Toshiaki Hayashi, Ritsuya Tomita, Yoshiro Hirayama, Science **312**, pages 1634 (2006)
 - ⁵³ Menghan Liao, Yunyi Zang, Zhaoyong Guan, Haiwei Li, Yan Gong, Kejing Zhu, Xiao-Peng Hu, Ding Zhang, Yong Xu, Ya-Yu Wang, Ke He, Xu-Cun Ma, Shou-Cheng Zhang and Qi-Kun Xue, Nature Phys **14**, 344–348 (2018). <https://doi.org/10.1038/s41567-017-0031-6>
 - ⁵⁴ Shu-Ping Lee, Karen Michaeli, Jason Alicea, and Amir Yacoby, Phys. Rev. Lett. **113**, 197001 (2014)
 - ⁵⁵ Sean Hart, Hechen Ren, Timo Wagner, Philipp Leubner, Mathias Mühlbauer, Christoph Brüne, Hartmut Buhmann, Laurens W. Molenkamp and Amir Yacoby, Nature Phys **10**, 638–643 (2014). <https://doi.org/10.1038/nphys3036>
 - ⁵⁶ Chenxiao Zhao, Leiqiang Li, Liying Zhang, Jin Qin, Hongyuan Chen, Bing Xia, Bo Yang, Hao Zheng, Shiyong Wang, Canhua Liu, Yaoyi Li, Dandan Guan, Ping Cui, Zhenyu Zhang, and Jinfeng Jia, Phys. Rev. Lett. **128**, 206802 (2022)
 - ⁵⁷ Xiao-Chuan Wu, Yichen Xu, Chao-Ming Jian, and Cenke Xu, Phys. Rev. B **100**, 155138 (2019).
 - ⁵⁸ Yi-Zhuang You and Ashvin Vishwanath, npj Quantum Materials **4**, 16 (2019)
 - ⁵⁹ Petr Stepanov, Ming Xie, Takashi Taniguchi, Kenji Watanabe, Xiaobo Lu, Allan H. MacDonald, B. Andrei Bernevig, and Dmitri K. Efetov, Phys. Rev. Lett. **127**, 197701, (2021).
 - ⁶⁰ Ipsita Das, Xiaobo Lu, Jonah Herzog-Arbeitman, Zhi-Da Song, Kenji Watanabe, Takashi Taniguchi, B. An-

doi:10.1038/s41567-021-01111-1, Nature Physics **17**, 710–714 (2021).